AFCRL-71-0429

CONTROL OF RADAR SCATTERING BY REACTIVE LOADING

by

Joseph R. Mautz

Roger F. Harrington

Department of Electrical and Computer Engineering
Syracuse University
Syracuse, New York 13210

Contract No. F19628-68-C-0180
Project No. 5635
Task No. 563506
Work Unit No. 56350601

SCIENTIFIC REPORT NO. 13

August 1971

Contract Monitor: John F. McIlvenna
Microwave Physics Laboratory

Prepared for

AIR FORCE CAMBRIDGE RESEARCH LABORATORIES
AIR FORCE SYSTEMS COMMAND
UNITED STATES AIR FORCE
BEDFORD, MASSACHUSETTS 01730

ABSTRACT

A method for obtaining a desired radar scattering pattern by reactively loading a conducting body is given. The theory uses the concept of characteristic modes of a loaded body. Any desired real current can be resonated by reactive loads to make it the dominant mode current of that body. If no other mode is near resonance, the radar scattering pattern becomes nearly the same as the radiation pattern of the resonated current. A quality factor Q is defined as a measure of the broadband behavior of a scatterer. Procedures for computing the real currents having minimum Q, and maximum gain-quality ratio, are given. A pattern synthesis procedure is developed for obtaining the real current whose radiation field pattern is the least mean square approximation to a desired field pattern. The use of lumped loads to approximate continuous loading is also considered. Numerical examples and computer programs are given for each procedure discussed.

CONTENTS

PART ONE

THEORY AND EXAMPLES

I. INTRODUCTION

A procedure for obtaining a desired electromagnetic scattering pattern by loading a conducting body is given in this report. Although primary concern is given to reactive loading, similar procedures can be applied to the more general case of impedance loading. It is well known that the radar cross section of a conducting body can be grossly changed by impedance loading [1]. This loading may be either continuous [2,3] or discrete [4,5]. Analyses are available for some specific cases, such as loaded wire dipoles [6,7] and loaded circular loops [8,9]. The problem of minimization of back scattering by loading has been considered for wire dipoles [10,11] and for wire loops [12].

Small conducting scatterers can be resonated by reactive loads to greatly enhance the scattered field [13]. The concept of resonance can be extended to larger conducting bodies through the use of characteristic modes [14-17]. Any desired real current can be resonated by reactive loads, thereby making that current the dominant mode current of the body. The scattering pattern then becomes predominantly that of the resonated mode, that is, of the desired real current. This assumes that the resonated mode is excited, and that no other mode is near resonance. The latter condition is usually met by bodies of electrically small and intermediate size, but may be violated if the body is electrically large. The resonance procedure tends to increase the scattered field of a body, and thus is more appropriate for cross section enhancement than for reduction.

Computation of mode currents and fields for reactively loaded surfaces is basically the same as for conducting surfaces [17,18]. Computer programs are available for surfaces of revolution [19] and for wire objects [20]. The computations included in this report are all for wire objects, although similar computations for surfaces of revolution have also been made.

II. MODES OF A LOADED SURFACE

A loaded surface S is defined as one for which the tangential electric field $\vec{E}_{tan}$ on S is related to the surface current $\vec{J}$ on S by an impedance function Z_L, that is

$$\vec{E}_{tan} = Z_L(\vec{J}) \tag{1}$$

The total electric field is the sum of the impressed field $\vec{E}^i$ plus the scattered field $\vec{E}^s$, produced by the currents $\vec{J}$ on S. In terms of vector and scalar potentials, the tangential component of E^s on S is given by [16]

$$\vec{E}^s_{tan} = (-j\omega\vec{A} - \vec{\nabla}\phi) = - Z(\vec{J}) \tag{2}$$

where the Z is called the impedance operator characterizing the surface. Letting $\vec{E} = \vec{E}^i + \vec{E}^s$, and substituting from (2) into (1), we have

$$(Z + Z_L)(\vec{J}) = \vec{E}^i_{tan} \tag{3}$$

This is the fundamental operator equation for the current J on a loaded surface excited by an incident field $\vec{E}^i$. It is of the same form as for conducting surfaces except that the operator $(Z + Z_L)$ in (3) replaces the operator Z in [16, eq. 7].

Modal solutions to (3) are obtained by a procedure similar to that used for conducting surfaces [16]. Consider the eigenvalue equation

$$(Z + Z_L)(\vec{J}_n) = \nu_n M(\vec{J}_n) \tag{4}$$

where ν_n are eigenvalues, $\vec{J}_n$ are eigenfunctions, and M is a weight operator to be chosen. In general,

$$Z = R + jX\ , \qquad Z_L = R_L + jX_L \tag{5}$$

where R and X are the Hermitian parts of Z, and R_L and X_L are the Hermitian parts of Z_L. If the loads are lossy, that is, if $R_L \neq 0$, we have two choices: (a) Set $M = R + R_L$, in which case the mode currents are real, but we lose orthogonality of the radiation patterns. (b) Set M = R, in which case we

retain orthogonality of the radiation patterns, but the mode currents may be complex.

For this report, we consider only reactive loads, that is, $R_L = 0$. The surface is loss free, and the above two choices for M become the same. Hence, let $M = R$ and $\nu_n = 1+j\lambda_n$ in (4), cancel the common terms $R(\vec{J}_n)$, and obtain

$$(X + X_L)(\vec{J}_n) = \lambda_n R(\vec{J}_n) \tag{6}$$

This is of the same form as for conducting surfaces, except that the operator $(X + X_L)$ in (6) replaces the operator X in [16, eq. (13)]. Now all properties of the mode currents and mode fields for the reactively loaded surface remain the same as for the conducting surface [16]. Some of the more important of these are:

(a) All eigenvalues λ_n and characteristic currents $\vec{J}_n$ are real. (More generally, the characteristic currents are equiphasal, that is, a complex constant times a real current.)

(b) The eigencurrents $\vec{J}_n$ form an orthogonal set with respect to the operator R over the surface S, that is,

$$\oiint_S \vec{J}_m \cdot R\vec{J}_n ds = 0 , \qquad m \neq n \tag{7}$$

(c) The eigencurrents $\vec{J}_n$ form an orthogonal set with respect to the operator $(X + X_L)$ over the surface S, that is,

$$\oiint_S \vec{J}_m \cdot (X + X_L)\vec{J}_n ds = 0 , \qquad m \neq n \tag{8}$$

(d) The eigenfields $\vec{E}_n$ (produced by $\vec{J}_n$) form an orthogonal set over the sphere at infinity S_∞, that is

$$\frac{1}{\eta} \oiint_{S_\infty} \vec{E}_m \cdot \vec{E}_n^* ds = 0 , \qquad m \neq n \tag{9}$$

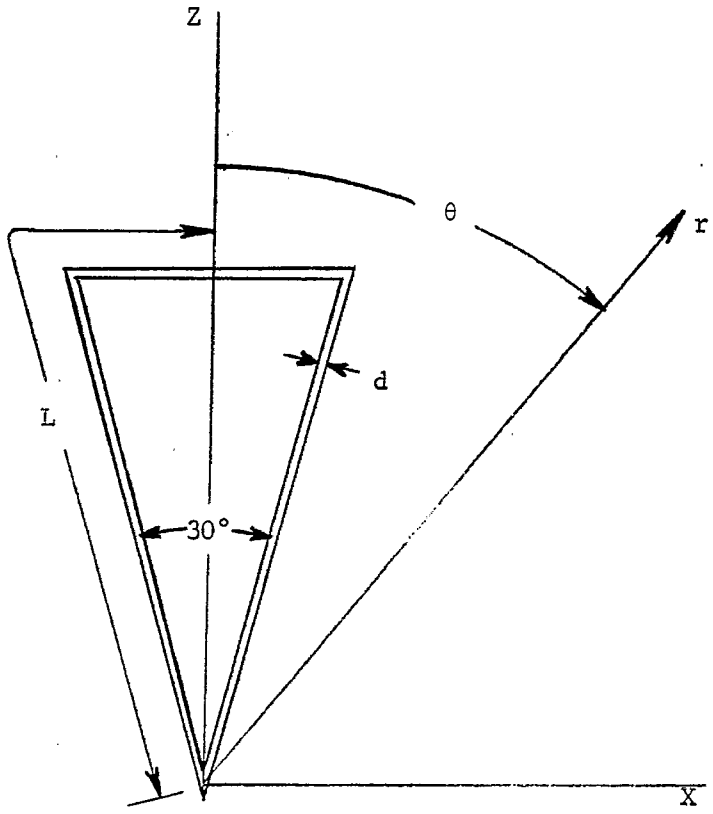

Fig. 1. Thin wire triangle used for illustrative computations.

(* denotes conjugate). The use of characteristic modes for radiation and scattering problems remains the same for reactively loaded surfaces as for conducting surfaces [16], except for minor changes due to replacing X by $(X + X_L)$. Formulas for the computation of modes and modal solutions for reactively loaded surfaces remain the same as for conducting surfaces [19], except that the generalized impedance matrix [Z] is replaced by $[Z + jX_L]$, where $[jX_L]$ is the load matrix.

It should be emphasized that the modes of a reactively loaded surface are different from those of the same surface unloaded. For illustrative purposes, we include computations for an unloaded ($X_L = 0$) thin wire triangle, as defined by Fig. 1. The half-length of the wire is L=one half wavelength, and the wire diameter d = 0.01L. The triangle lies in the y=0 plane with tip at the origin. The coordinates of a field point are the usual r,θ,ϕ spherical coordinates. All computations are made with a Galerkin solution using 30 triangle functions for expansion of the current [18,20]. Hence, the generalized impedance matrix for the wire was 30 by 30 in size. The four lowest order mode currents for the unloaded wire triangle are shown in Fig. 2. The four lowest order mode gain patterns for the unloaded wire triangle are shown in the x=0 plane in Fig. 3, and in the y=0 plane in Fig. 4. Convergence of the modal solution for bistatic radar cross section, given a plane wave axially incident on the 30° angle of the unloaded triangle, is illustrated by Fig. 5. Those modes excited by the plane wave (even symmetry) are added in the order of increasing $|\lambda_n|$. Note that only two modes contribute significantly to the scattering pattern.

III. RESONATING A DESIRED REAL CURRENT

The modal solution for the field scattered by a reactively loaded surface is of the same form as for a conducting surface [16, eq. 31]

$$\vec{E}^s = \sum_n \frac{V_n^i \vec{E}_n}{1+j\lambda_n} \tag{10}$$

where $\vec{E}_n$ are the mode fields and V_n^i is the mode excitation coefficient

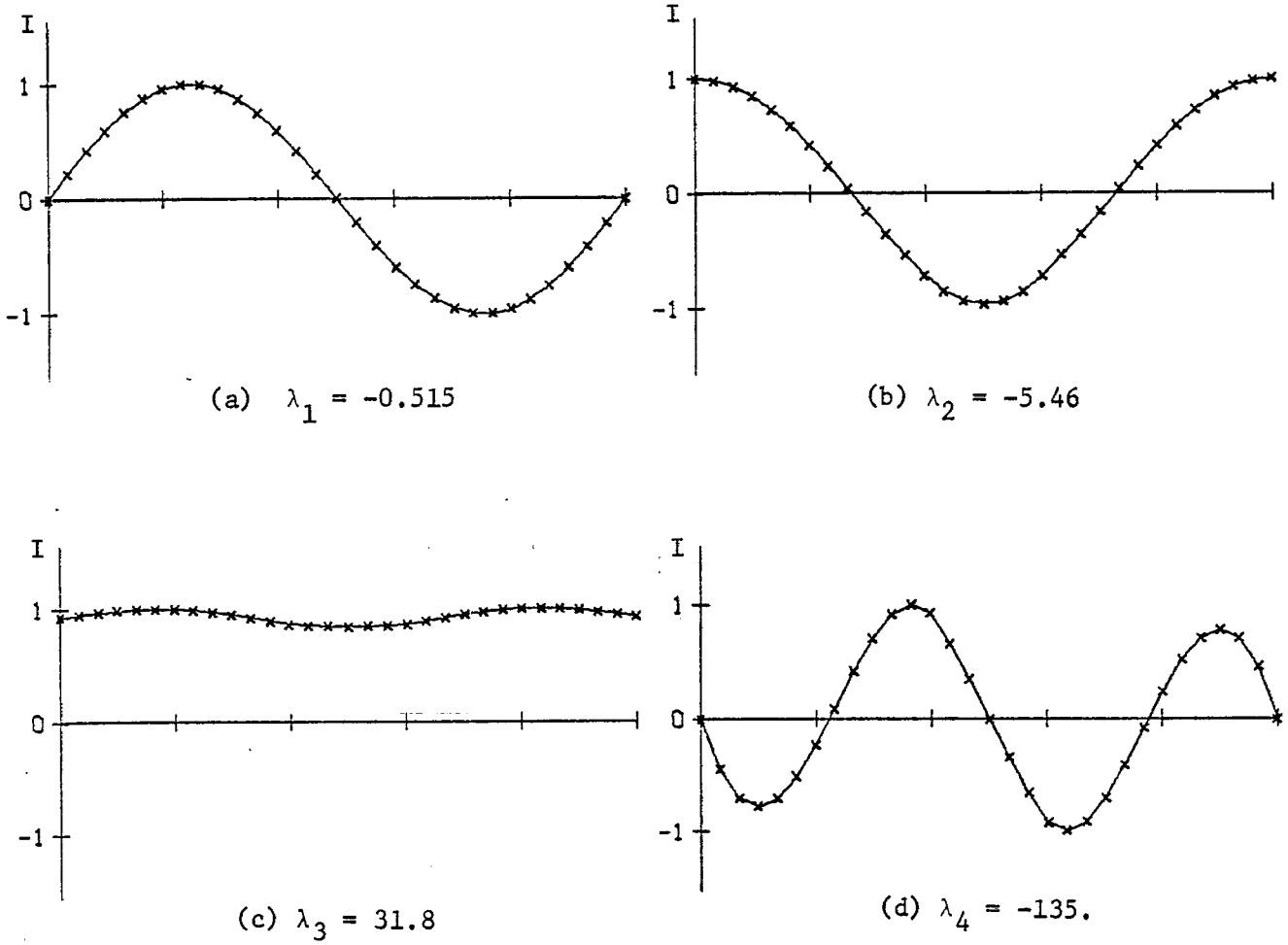

Fig. 2. Lowest order mode currents for the unloaded wire triangle of Fig. 1.

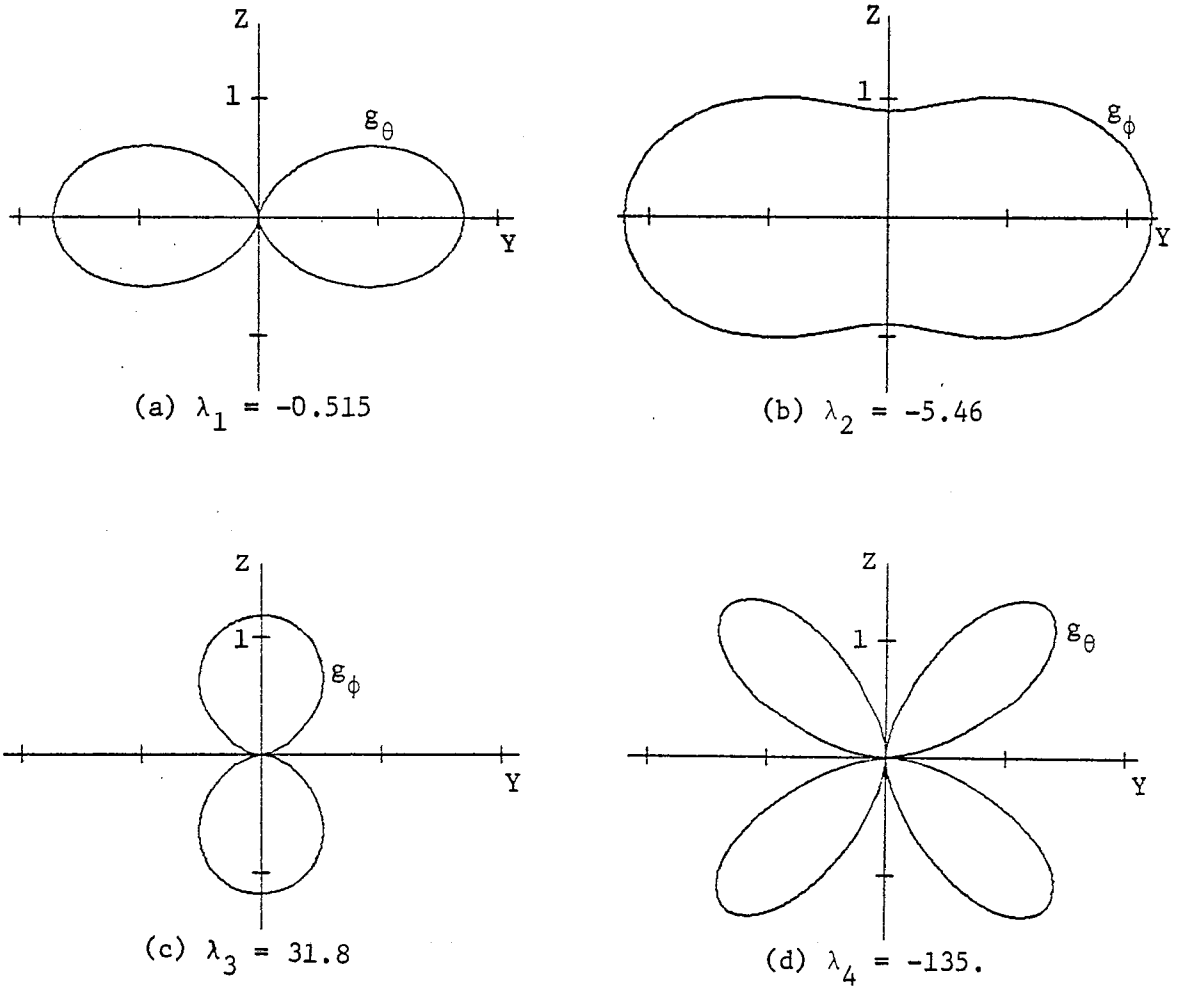

Fig. 3. Lowest order mode gain patterns in the x=0 plane for the unloaded wire triangle of Fig. 1. (Subscript on g denotes polarization of the field.)

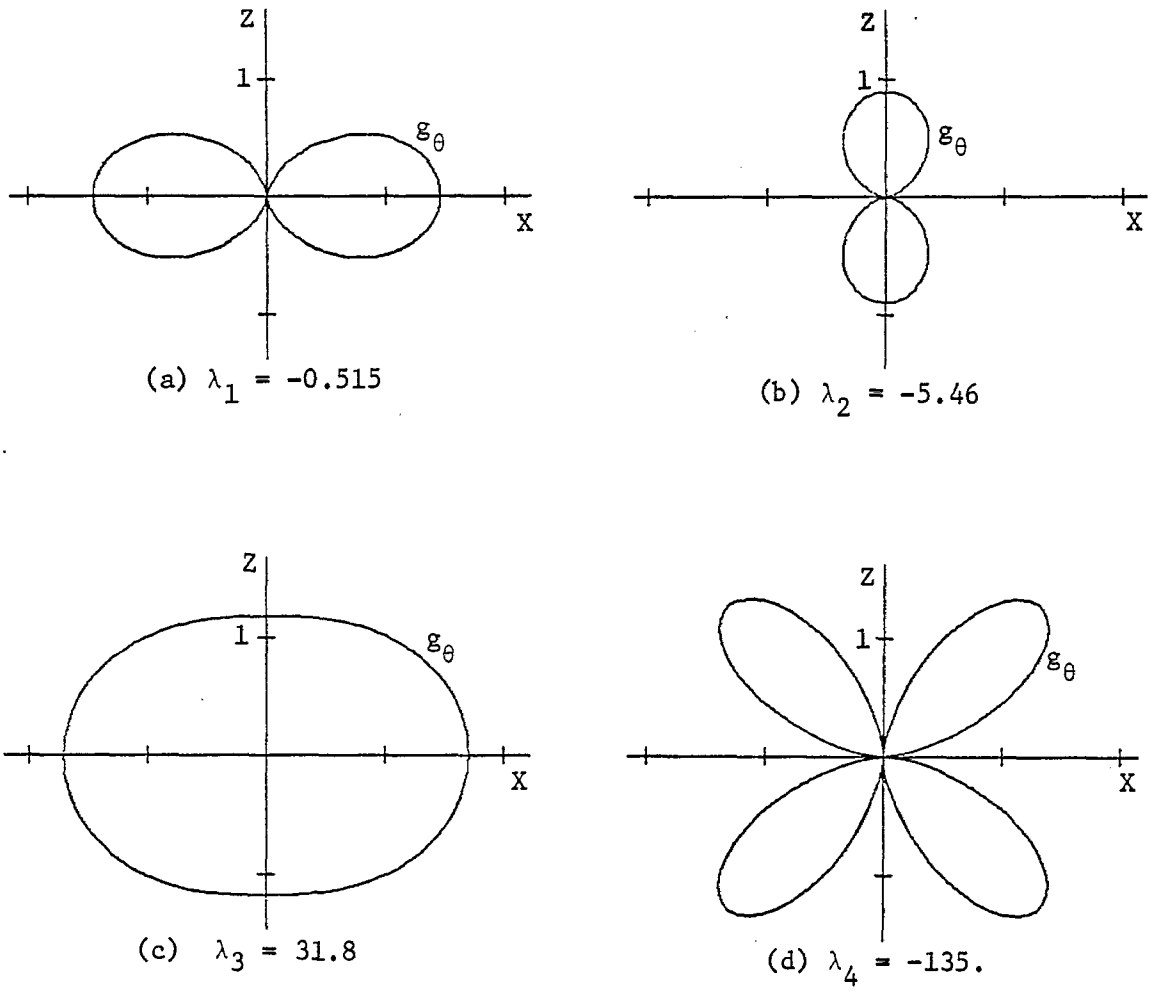

Fig. 4. Lowest order mode gain patterns in the y=0 plane for the unloaded wire triangle of Fig. 1. (Subscript on g denotes polarization of the field.)

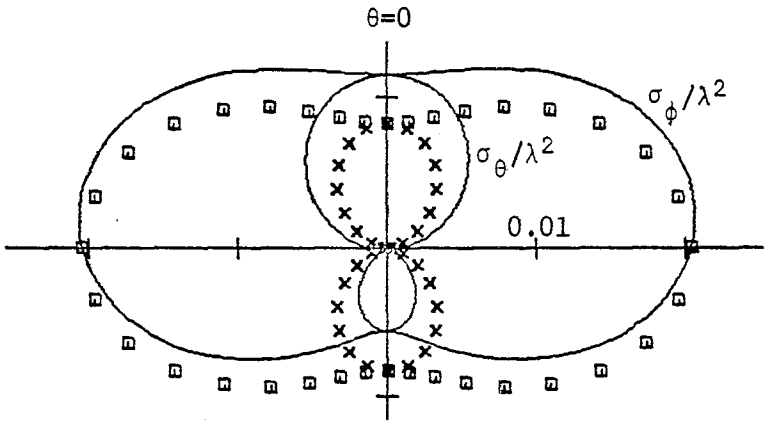

(a) $\lambda_1 = -0.515$

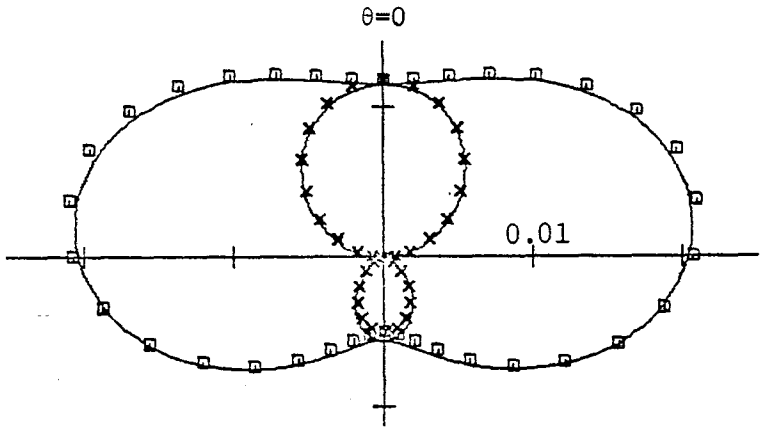

(b) add $\lambda_3 = 31.8$

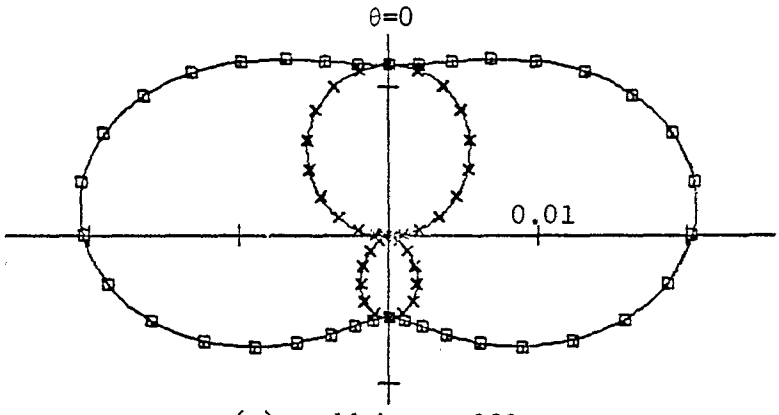

(c) add $\lambda_5 = -282$

Fig. 5. Convergence of the modal solution for bistatic radar cross section/wavelength squared (σ/λ^2) for the unloaded wire triangle excited by a plane wave axially incident on the 30° angle. Modes are added in the order of increasing $|\lambda_n|$. Patterns in the x=0 plane are plotted by squares, in the y=0 plane by x's. Solid curves are the matrix inversion solution.

$$V_n^i = \oint\!\!\oint_S \vec{J}_n \cdot \vec{E}^i_{tan} ds \tag{11}$$

The modes which contribute most to $\vec{E}^s$ are those having the smallest $|\lambda_n|$, under the assumption that they are excited (V_n^i not zero). A mode having $|\lambda_n| = 0$ is said to be externally resonant. If no other $|\lambda_n|$ is also small, then the scattered field consists almost entirely of the single resonant mode field. This has been true for all electrically small and intermediate size scatterers for which we have performed computations.

For a reactively loaded surface, any real current $\vec{J}$ can be made an eigencurrent corresponding to the eigenvalue $\lambda=0$ by choosing the appropriate loading reactance. To show this, let

$$X_L(\vec{J}) = - X(\vec{J}) \tag{12}$$

whence the left-hand side of (6) is zero. If $\vec{J}$ is not associated with an internal resonance, $R(\vec{J}) = 0$ and the eigenvalue λ must be zero. Assuming X_L to be a simple function of proportionality, we can solve (12) for the required surface reactance on S.

The above procedure becomes clearer when expressed in matrix notation. To be explicit, consider a wire object and apply the method of moments with triangle functions for expansion and testing. Let s be the length variable along the wire, I(s) the current on the wire, and $T(s-s_i)$ a triangle function extending from point s_{i-1} to s_{i+1}, with unit peak at s_i. Then the current is given by

$$I(s) = \sum_i I_i \, T(s-s_i) \tag{13}$$

where $I_i = I(s_i)$ are unknown coefficients. Applying Galerkin's method to (3), we obtain the matrix equation [21]

$$[Z + Z_L][I] = [V^i] \tag{14}$$

where [I] is the column matrix of the I_i, $[V^i]$ is the excitation matrix with elements

$$V_j^i = \int_{\text{wire}} T(s-s_j)\, E_s^i(s)\, ds \tag{15}$$

[Z] is the generalized impedance matrix for the wire [22], and $[Z_L]$ is the load impedance matrix with elements

$$(Z_L)_{ij} = \int_{\text{wire}} ds \int_{\text{wire}} ds'\, T(s'-s_i)\, Z_L(s)\, T(s-s_j) \tag{16}$$

Note that $[Z_L]$ is at most a tridiagonal matrix, since Z_L is an ordinary function of position. To simplify computation, we approximate $Z_L(s)$ by lumped impedances at the points s_i, in which case $[Z_L]$ becomes a diagonal matrix. Computational checks show that this makes no noticeable difference in the solution so long as the s_i are close together. A solution for the current [I] is obtained from (14) by matrix inversion.

For our problem $[Z_L]$ is a pure reactance $[jX_L]$. Hence, the matrix representation of the eigenvalue equation (6) is

$$[X + X_L][I] = \lambda[R][I] \tag{17}$$

where $[X_L]$ is the diagonal matrix

$$[X_L] = \begin{bmatrix} X_{L1} & 0 & 0 & \cdots \\ 0 & X_{L2} & 0 & \cdots \\ 0 & 0 & X_{L3} & \cdots \\ \cdots & \cdots & \cdots & \cdots \end{bmatrix} \tag{18}$$

To resonate a desired real current [I], set the right-hand side of (17) equal to zero, and, analogous to (12), obtain

$$X_{Li} I_i = -\left([X][I]\right)_i \tag{19}$$

for i=1,2,3,... . The notation $([X][I])_i$ means the i-th element of the column matrix [X][I]. Since [X] and [I] (the desired current) are known, the reactive loads can be computed from (19).

To illustrate the procedure, suppose we want to resonate the $\lambda = 31.84$ mode current of the unloaded wire triangle, Fig. 1. This "desired current" is that of Fig. 2c, and its characteristic mode gain patterns are those of Figs. 3c and 4c. The reactances X_{Li} required at the 30 points s_i needed to resonate the current are computed according to (19). These loads are then added to the generalized impedance matrix as in (14), and the new mode currents and fields computed with available programs [20]. The four lowest order mode currents for the reactively loaded triangle are plotted in Fig. 6. Note that the new dominant mode current, for which $\lambda = -0.0002$, is identical to the third mode current of the unloaded triangle, for which $\lambda = 31.84$, as anticipated. The other mode currents for the loaded structure are different from those of the unloaded structure. The new mode gain patterns are not shown, but, except for the mode resonated, they are different from those of the unloaded structure. Convergence of the modal solution for bistatic radar cross section, given a plane wave axially incident on the 30° angle of the loaded triangle, is shown in Fig. 7. Note that the scattering pattern is almost identical to the mode pattern of the current resonated, Figs. 3c and 4c, as desired.

It can be shown that the gain pattern of any real current is "point-symmetric," that is, its gain in any direction $\hat{r}$ is equal to that in the opposite direction $-\hat{r}$. Whenever a scatterer is loaded to resonate a real current, its scattering pattern is also nearly point-symmetric, because the current is principally the real resonated current. The bistatic radar cross section pattern of Fig. 7 exhibits this point symmetry. As a corollary to this property, we can say that a scatterer loaded to resonate a real current has approximately equal forward scattering and back scattering cross sections.

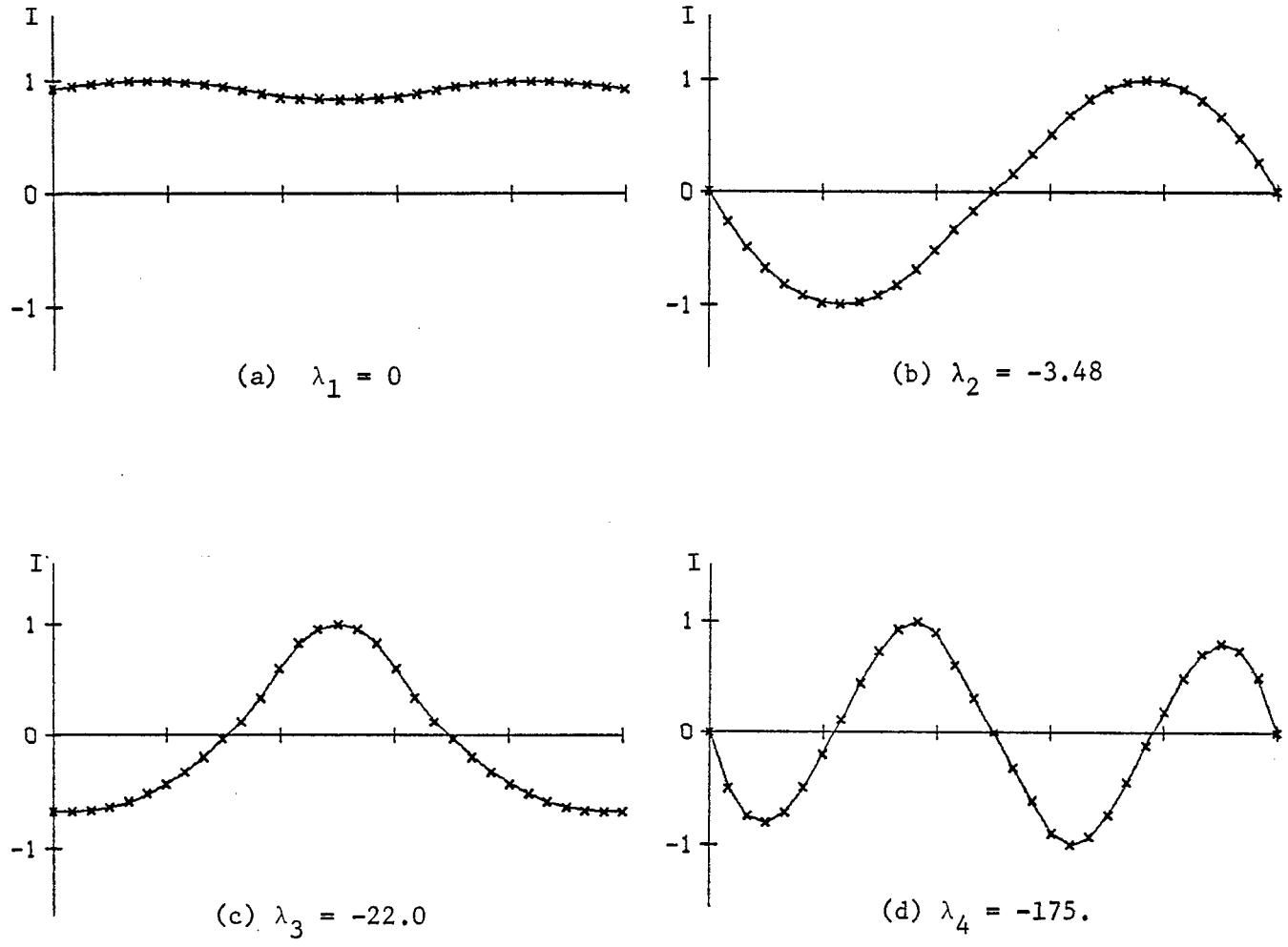

Fig. 6. Lowest order mode currents for the reactively loaded wire triangle of Fig. 1. Loads were chosen to resonate the $\lambda = 31.84$ mode current of the unloaded triangle.

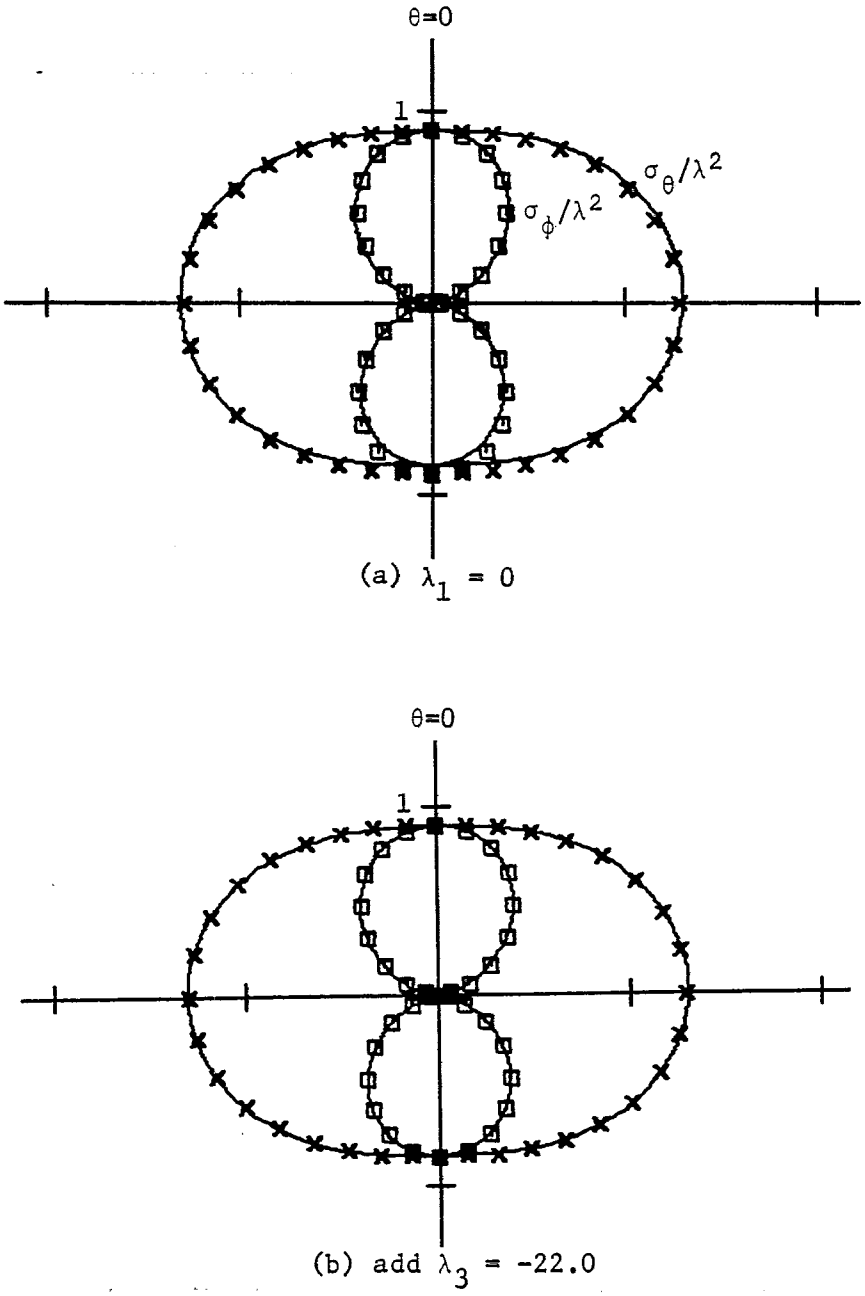

Fig. 7. Convergence of the modal solution for bistatic radar cross section/wavelength squared (σ/λ^2) for the reactively loaded wire triangle excited by a plane wave axially incident on the 30° angle. Modes are added in the order of increasing $|\lambda_n|$. Patterns in the x=0 plane are plotted by squares, in the y=0 plane by x's. Solid curves are the matrix inversion solution.

IV. BROADBAND SCATTERERS

It is often desirable to have a scatterer whose characteristics change slowly with frequency. As a measure of the frequency sensitivity of a current [I], we define its quality factor as

$$Q = \omega \frac{[\tilde{I}^*][X'][I]}{[\tilde{I}^*][R][I]} \tag{20}$$

where $[X'] = [dX/d\omega]$. If [I] is an eigencurrent, an interpretation of Q can be made in terms of the frequency variation of the eigenvalue, as follows. Consider the Rayleigh quotient formula for λ, and assume that the dominant frequency variation is due to that of [X]. Taking the frequency derivative of the Rayleigh quotient, we have

$$Q \approx \omega \frac{\partial \lambda}{\partial \omega} \tag{21}$$

A scatterer will be called broadband if only low Q modes contribute significantly to the scattered field.

The reader may note that the Q defined by (20) differs from that previously defined for small antennas [21, eq. (10-81)]. Since the electric and magnetic energies [21, eq. (10-79)] must be positive, it follows that

$$\omega[\tilde{I}^*][X'][I] \geq [\tilde{I}^*][X][I] \tag{22}$$

Hence, for electrically small antennas, the Q of (20) is always greater than or equal to that previously defined. In other words, for electrically small antennas,

$$Q \geq \frac{1}{\beta} \tag{23}$$

where β is the fractional bandwidth of the input impedance to the antenna.

The lowest Q currents for a given surface can be found from the Rayleigh quotient (20) in the usual way [21]. The resulting eigenvalue equation is

$$[\omega X'][I] = Q[R][I] \tag{24}$$

where Q is the eigenvalue. The smallest eigenvalue is the minimum Q for all possible currents [I]. Equation (24) has been solved for the wire triangle

of Fig. 1, and the lowest order Q found to be Q = 7.38. The corresponding current is shown in Fig. 8a, and the gain patterns in the x=0 and y=0 planes are shown in Fig. 9a. The current is an odd function about the midpoint of the length variable, and it radiates maximum field in the z=0 plane. We call it a broadside mode. The next lowest Q was Q = 27.6. The corresponding current is shown in Fig. 8b, and the gain patterns in the x=0 and y=0 planes are shown in Fig. 9b. Note that this current is an even function about the midpoint of the length variable, and it radiates maximum field in the z direction. We call this current the lowest Q endfire current.

We next choose the lowest Q endfire current as the one to resonate according to the concepts of Section III. The required load reactances are found from (19), and the modes of the loaded triangle calculated by the programs of [20]. The four lowest order mode currents are shown in Fig. 10. Note that the higher order modes have a jump at the points where the dominant mode current has a zero. This is because the load at this point is a very large reactance, almost an open circuit. The dominant mode current is the lowest Q endfire current, Fig. 8b. All mode currents are all different from those for the unloaded triangle, Fig. 2. Convergence of the modal solution for the bistatic radar cross section, given a plane wave axially incident on the 30° angle of the loaded triangle, is illustrated by Fig. 11. The solution is essentially only one mode, that of the resonated lowest Q endfire current, hence only one plot is shown in Fig. 11. Note that the scattering patterns are identical to the mode patterns, Fig. 9b. Note also that these mode patterns are similar to those of a magnetic dipole, which agrees with our intuition that low Q currents are associated with dipole fields.

To illustrate the variation of radar cross section over a frequency band, graphs of backscattering cross section versus frequency are shown in Fig. 12. The object is a wire angle-circle (cross section of a cone-sphere) with various loads. As shown in the insert of Fig. 12, it consists of a 12° wire angle closed by a wire circle of 8 inches outside diameter. The wire diameter is one-tenth the circle diameter. This object is naturally resonant in the vicinity of 175 MHz. The wire is excited by a plane wave axially incident on the angle. Curve (a) shows σ/λ^2 for the unloaded wire, curve (b)

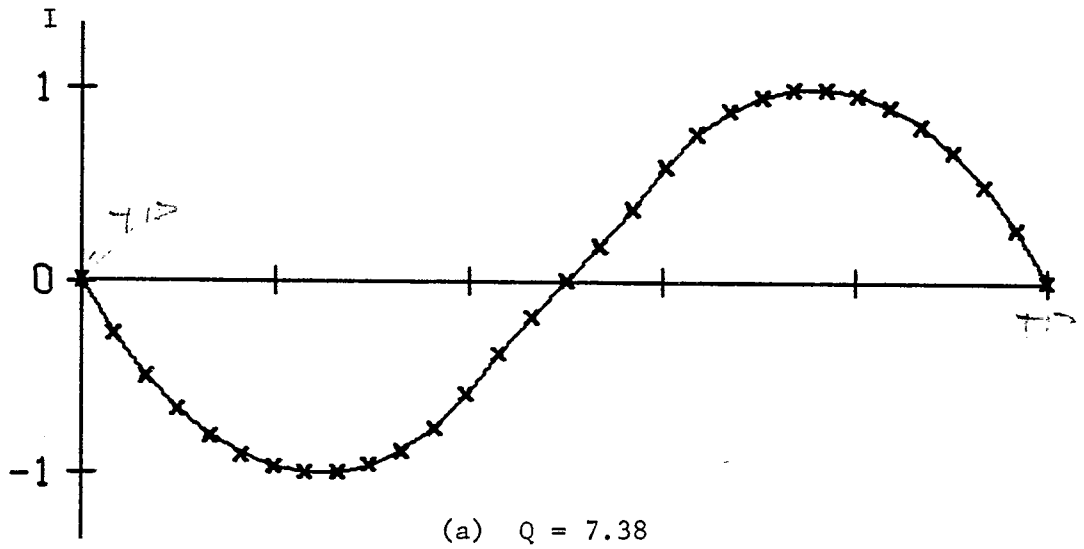

(a) Q = 7.38

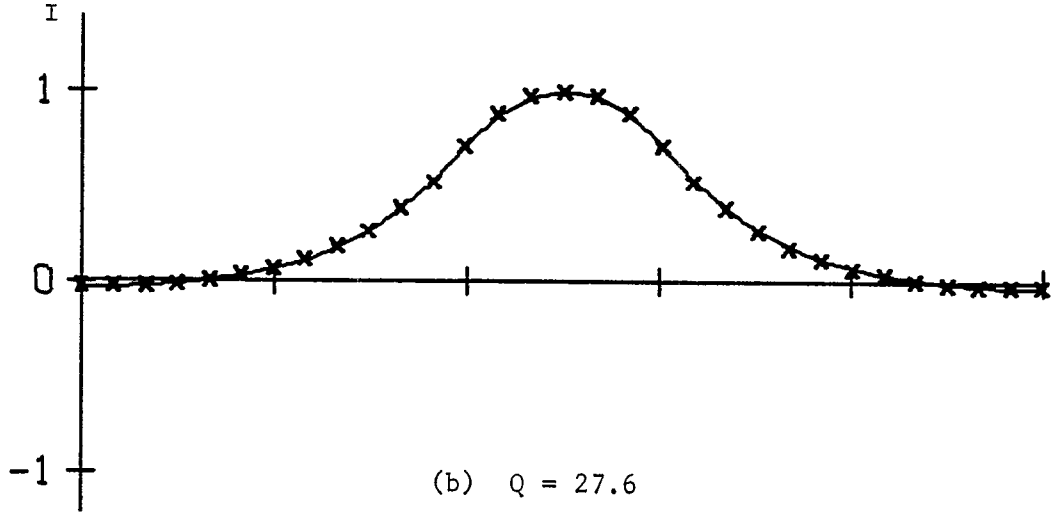

(b) Q = 27.6

Fig. 8. Lowest Q currents for the wire triangle of Fig. 1.
(a) Lowest Q odd current (broadside radiation).
(b) Lowest Q even current (endfire radiation).

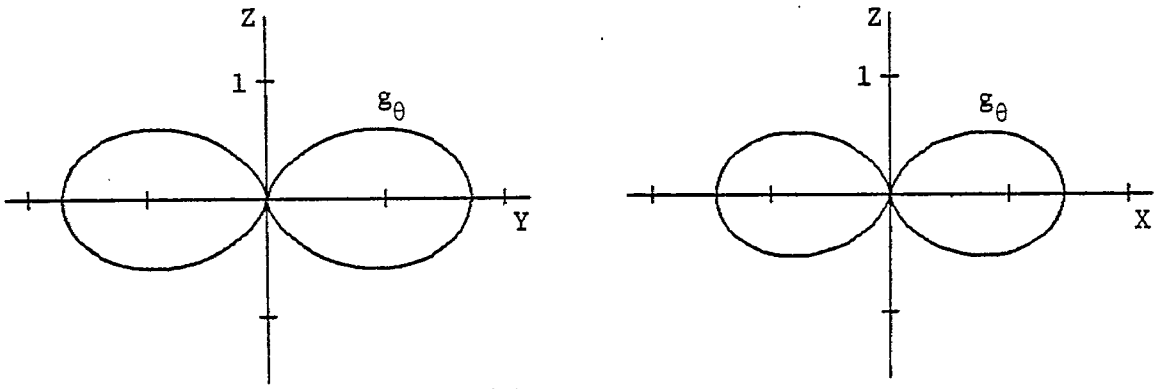

(a) Q = 7.38

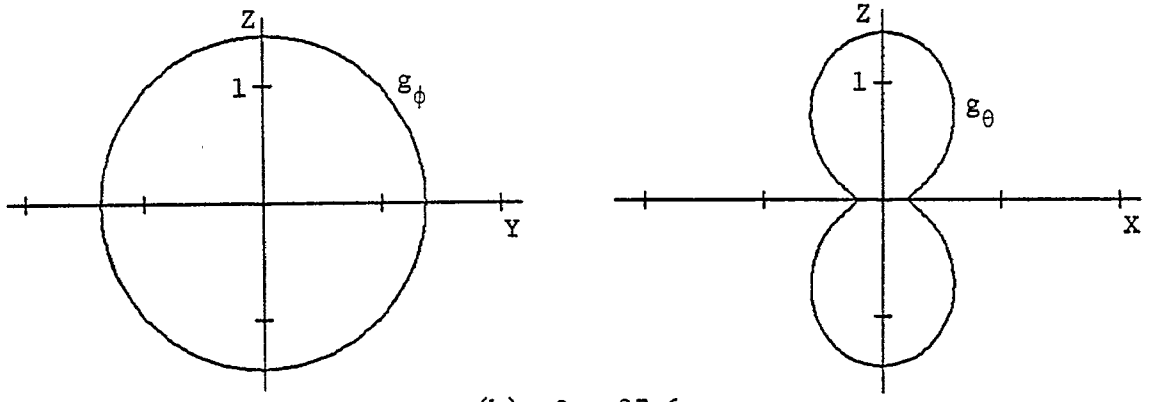

(b) Q = 27.6

Fig. 9. Gain patterns for the lowest Q currents of the wire triangle of Fig. 1. (a) Lowest broadside Q. (b) Lowest end-fire Q.

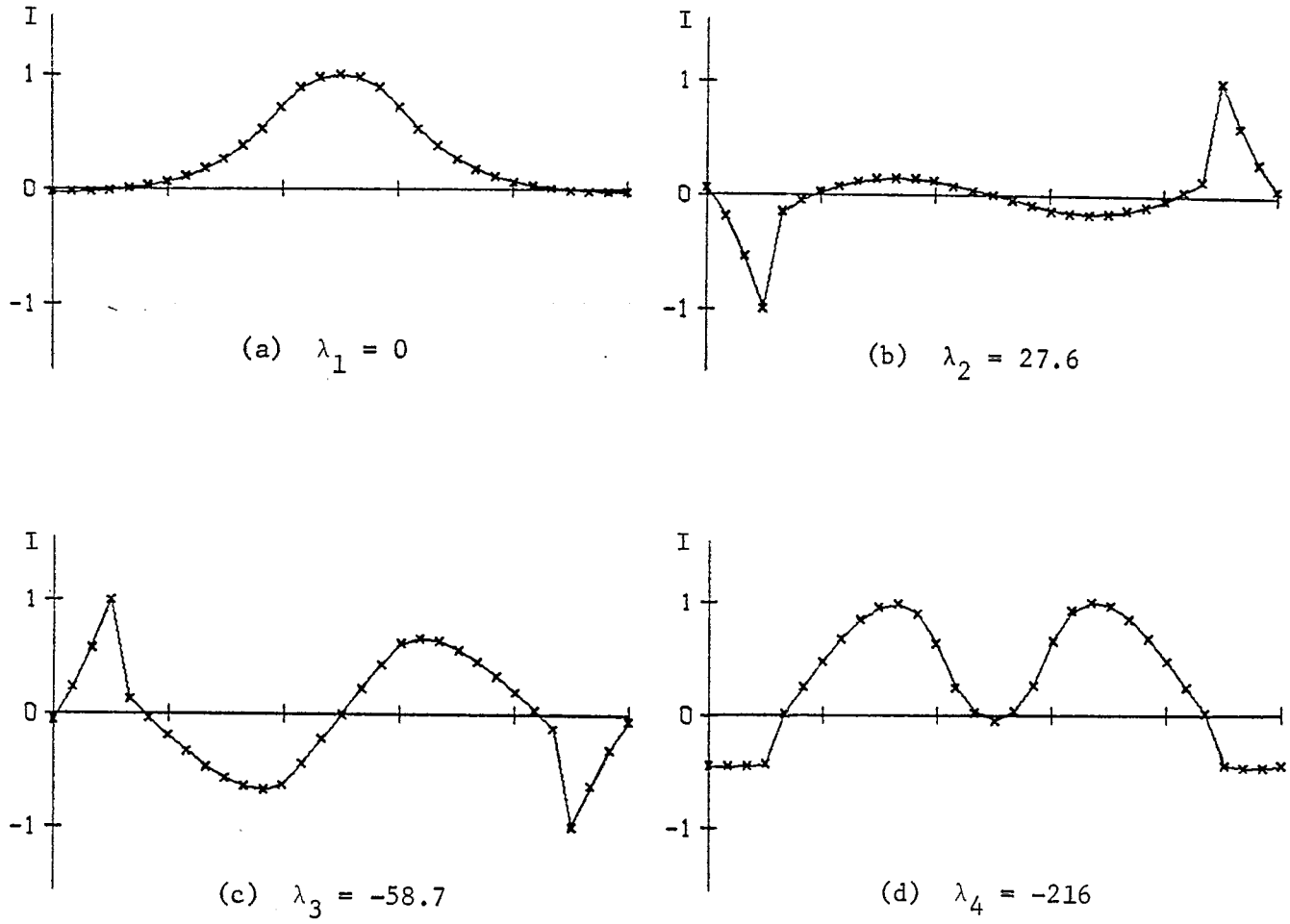

Fig. 10. Lowest order mode currents for the wire triangle reactively loaded to resonate the lowest Q endfire current.

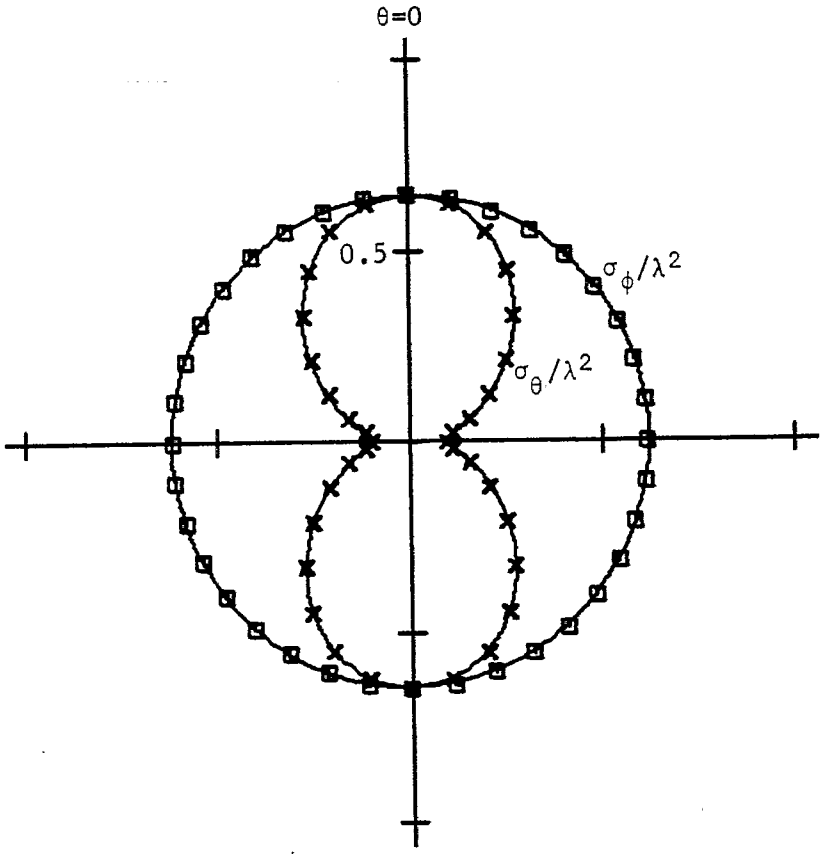

Fig. 11. Modal solution compared to the matrix inversion solution (solid) for bistatic radar cross section/ wavelength squared (σ/λ^2) for the triangle reactively loaded to resonate the lowest Q endfire mode, and excited by a plane wave incident on the 30° angle. Patterns in the x=0 plane are plotted by squares, in the y=0 plane by x's.

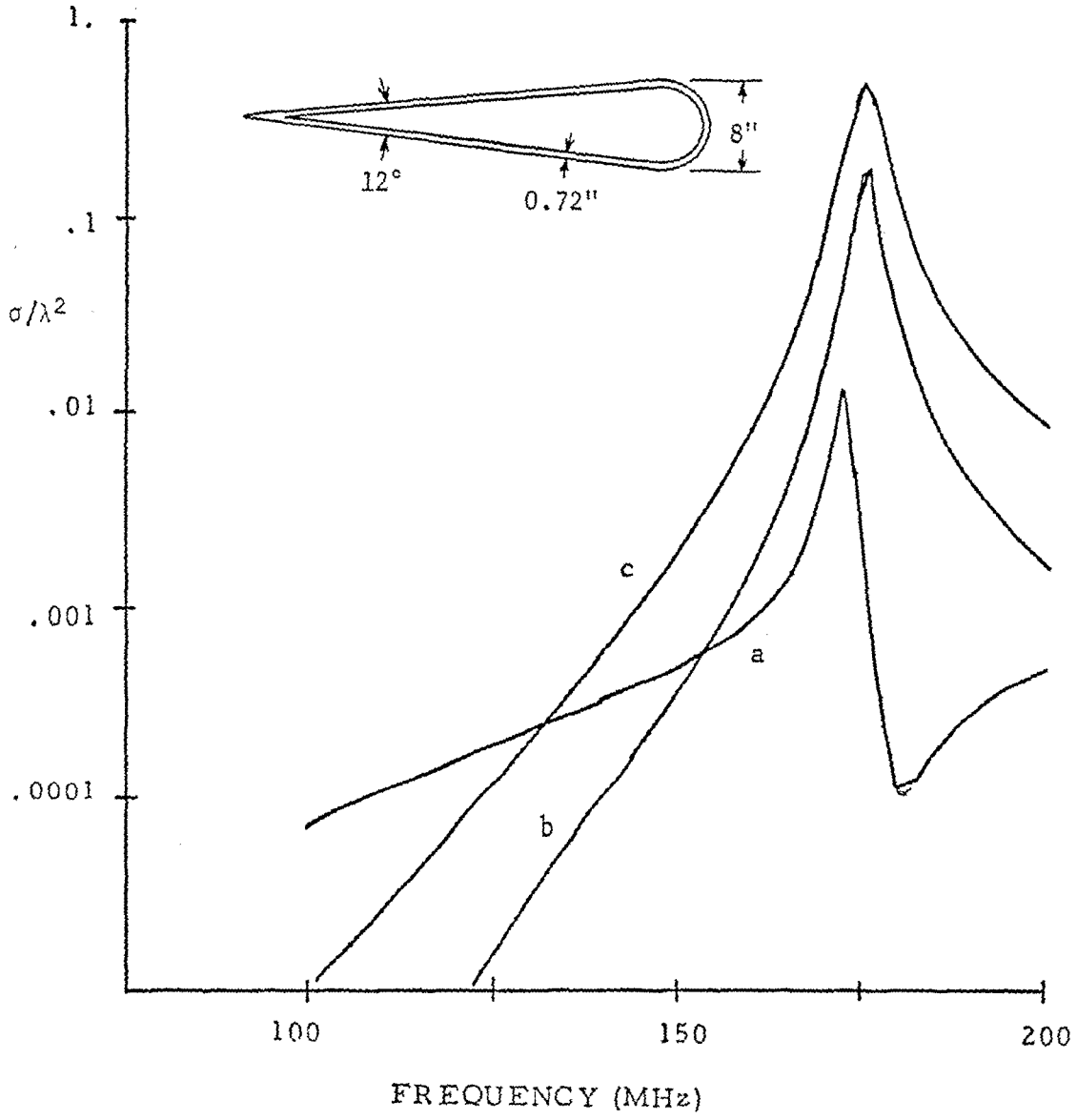

Fig. 12. Back scattering radar cross section/wavelength squared (σ/λ^2) versus frequency for a wire angle-circle (cross section of a cone-sphere). (a) Unloaded wire. (b) Wire loaded to resonate the most inductive eigencurrent of the unloaded wire. (c) Wire loaded to resonate the lowest Q endfire current.

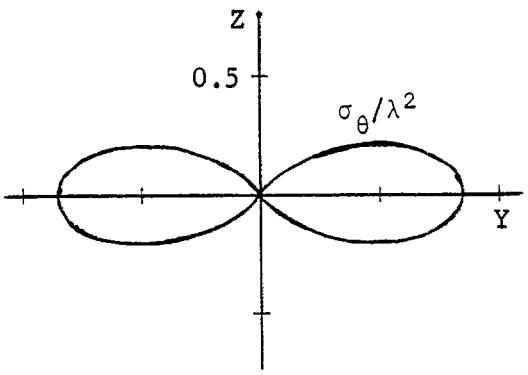

(a) Unloaded (x=0 plane)

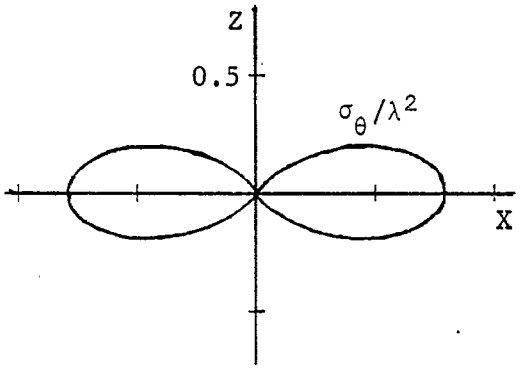

(b) Unloaded (y=0 plane)

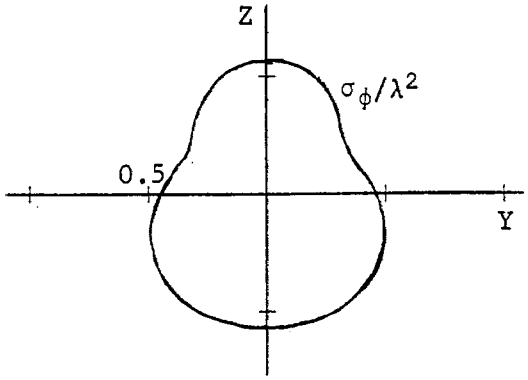

(c) Loaded (x=0 plane)

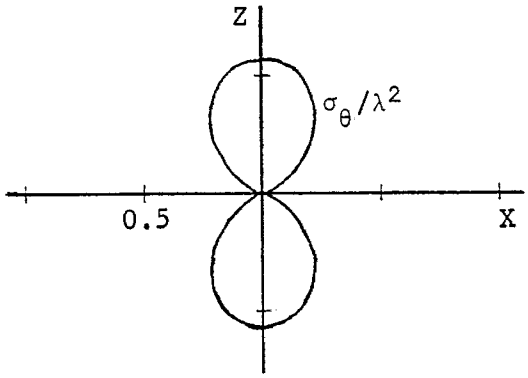

(d) Loaded (y=0 plane)

Fig. 13. Comparison of the monostatic radar cross sections of the unloaded angle-circle with those for the angle-circle loaded to resonate the lowest Q endfire current at a frequency of 150 MHz.

shows σ/λ^2 for the wire loaded to resonate the most inductive eigencurrent (largest positive λ_n) of the unloaded wire, and curve (c) shows σ/λ^2 for the wire loaded to resonate the lowest Q endfire current. Note that the lowest Q case is considerably more broadband than the other two.

Finally, to illustrate the gross changes in radar cross section that can be obtained by reactive loading, Fig. 13 shows the directional variation of backscattering cross section at 150 MHz for the unloaded wire angle-circle and for the wire loaded to resonate the lowest Q endfire current. The angle-circle is that shown in the insert of Fig. 12. Figure 13a shows σ/λ^2 (θ polarization) in the x=0 plane for the unloaded wire, and Fig. 13b shows σ/λ^2 (θ polarization) in the y=0 plane for the same unloaded wire. Figure 13c shows σ/λ^2 (ϕ polarization) in the x=0 plane for the wire loaded to resonate the lowest Q endfire mode and Fig. 13d shows σ/λ^2 (θ polarization) in the y=0 plane for the same loaded wire. Note that the wire angle-circle has been changed from a broadside scatterer to an endfire scatterer by the introduction of reactive loads.

V. MAXIMUM GAIN-QUALITY RATIO

The power gain of a system of currents is defined as the ratio of the radiation intensity in a given direction and polarization to the radiation intensity which would be obtained if all power were radiated omnidirectionally. In terms of matrix elements, it is given by [21]

$$G = \frac{k^2 \eta}{4\pi} \frac{[\tilde{I}^*][V^*][\tilde{V}][I]}{[\tilde{I}^*][R][I]} \tag{25}$$

where k is the wavenumber, η is the intrinsic impedance of space, and [V] is the voltage excitation column matrix due to a unit plane wave incident from the measurement direction. By dividing (25) by (20), we have the gain-quality ratio

$$\frac{G}{Q} = \frac{k^2 \eta}{4\pi\omega} \frac{[\tilde{I}^*][V^*][\tilde{V}][I]}{[\tilde{I}^*][X'][I]} \tag{26}$$

If the reciprocal of Q is interpreted as bandwidth, then (26) is also known as the gain-bandwidth product.

The parameter G/Q is in the form of a Rayleigh quotient, hence its stationary points are the eigenvalues of

$$\frac{k^2\eta}{4\pi\omega}\,[V^*][\tilde{V}][I] = \frac{G}{Q}\,[X'][I] \tag{27}$$

Since $[V^*][\tilde{V}]$ is a one-term dyad, all eigenvalues of (27) are zero except one, which is

$$\left(\frac{G}{Q}\right)_o = \frac{k^2\eta}{4\pi\omega}\,[\tilde{V}][X']^{-1}[V^*] \tag{28}$$

The associated eigenvector is

$$[I]_o = [X']^{-1}[V^*] \tag{29}$$

or any constant times it. For currents of electrically small extent it can be shown that [X'] is positive definite, in which case $(G/Q)_o$ is the maximum gain-quality ratio. For currents of electrically large extent, [X'] may be indefinite, in which case $(G/Q)_o$ is merely a stationary point. However, it still defines a current $[I]_o$ which is relatively insensitive to frequency variation and therefore of value in the design of broadband scatterers.

A current can be a mode current only if it is equiphasal, that is, a real current times a complex constant. Since the complex constant cancels in (25), it is sufficient to consider [I] to be real. Hence, we reconsider the optimization procedure with [I] restricted to the real field. The details for general problems of this type are given in the Appendix. The results specialized to our particular problem are as follows. For [I] real, the non-zero stationary points of G/Q are given by

$$\left(\frac{G}{Q}\right)_r = \frac{k^2\eta}{4\pi\omega}\,\mathrm{Re}[\tilde{V}][X']^{-1}\,(\mathrm{Re}[V] + c\,\mathrm{Im}[V]) \tag{30}$$

where c has the two values

$$c = -a \pm \sqrt{a^2 + 1} \tag{31}$$

and

$$a = \frac{\mathrm{Re}[\tilde{V}][X']^{-1}\mathrm{Re}[V] - \mathrm{Im}[\tilde{V}][X']^{-1}\mathrm{Im}[V]}{2\ \mathrm{Re}[\tilde{V}][X']^{-1}\mathrm{Im}[V]} \tag{32}$$

Here Re[V] and Im[V] denote the real and imaginary parts of the complex column vector [V]. If [X'] is positive definite, the larger of the two values G/Q obtained from (30) will be the maximum obtainable with real current. The current corresponding to the stationary points (30) is

$$[I] = [X']^{-1}(\mathrm{Re}[V] + c\ \mathrm{Im}[V]) \tag{33}$$

It is shown in the Appendix that the maximum G/Q for real current is at least one-half of that attainable for complex current. The two cases are equal if [V] is equiphasal.

To illustrate typical results, consider the wire triangle of Fig. 1, and let G/Q be maximized for some direction θ_o in the y=0 plane (plane of the triangle). Figure 14 shows the real current for maximum G/Q in the directions (a) $\theta_o = 0$ (endfire), (b) $\theta_o = 20°$, (c) $\theta_o = 45°$, and (d) $\theta_o = 90°$ (broadside). Note that, as θ_o is increased from 0 to 90°, the current changes gradually from an endfire current to a broadside current. Note also that the maximum G/Q currents, Fig. 14a and d, differ somewhat from the minimum Q currents, Figs. 8b and 8a, respectively. The gain patterns for the currents of Fig. 14 are shown in Figs. 15 and 16. Those of Fig. 15 are in the y=0 plane and θ polarized. Those of Fig. 16 are in the x=0 plane, with (a) and (b) ϕ polarized, and (c) and (d) θ polarized. In case (b) there is also a small θ polarized field (not shown), and in case (c) there is also a small ϕ polarized field (not shown). Finally, the real currents of Fig. 14 can be resonated by reactive loads according to the concepts of Section III. When the loaded wire object is excited by a plane wave from or near θ_o, the bistatic radar cross Section patterns consist primarily of the resonated mode. Hence, the radar cross section patterns are essentially the same as the patterns of Figs. 15 and 16, except for a scale change.

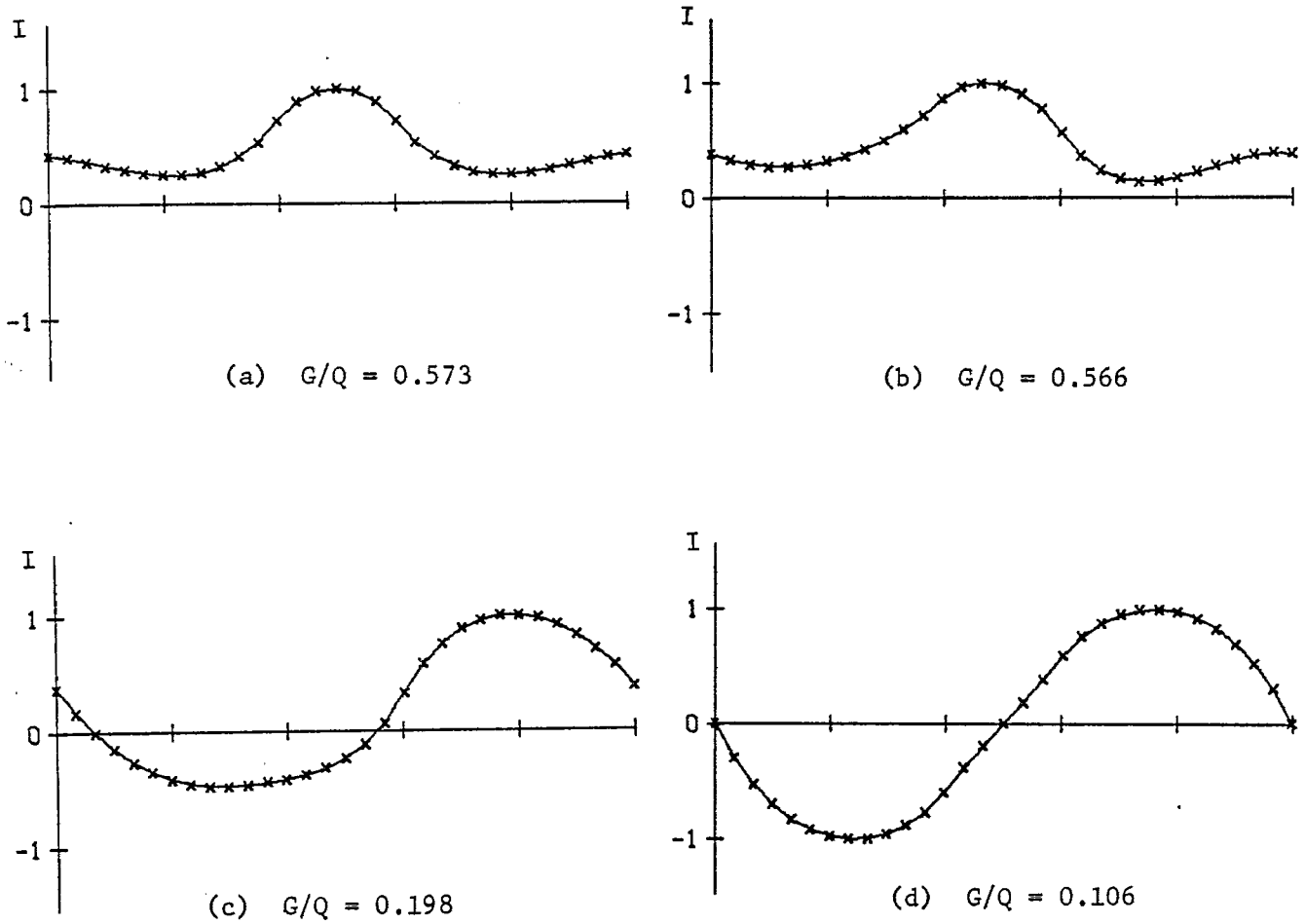

Fig. 14. Real currents for maximum G/Q for the wire triangle of Fig. 1. Gain is taken in the y=0 plane at the angles (a) $\theta_o = 0$ (endfire), (b) $\theta_o = 20°$, (c) $\theta_o = 45°$, and (d) $\theta_o = 90°$ (broadside).

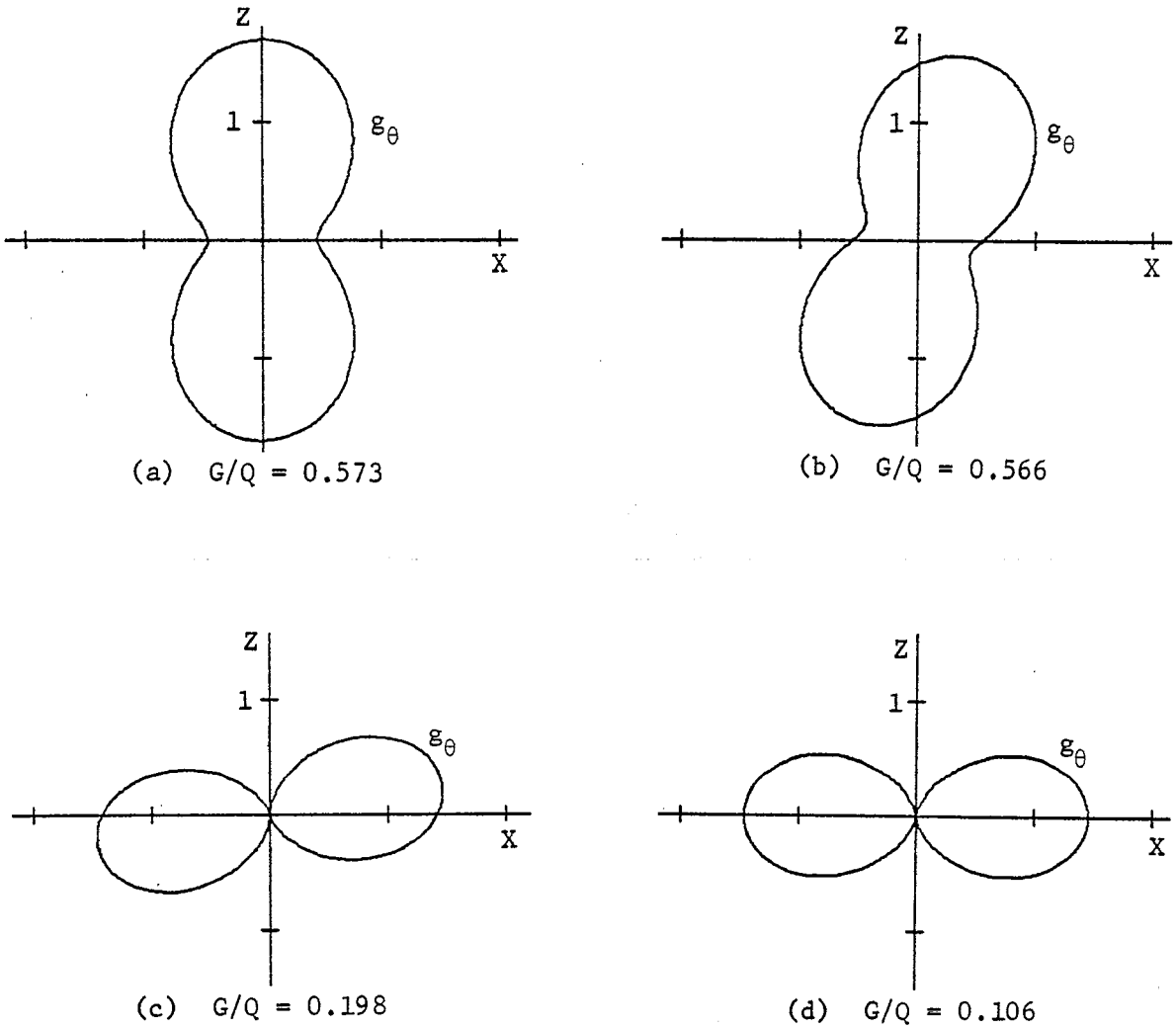

Fig. 15. Gain patterns for the maximum G/Q currents of Fig. 14 in the plane of the triangle (y=0). Field is θ-polarized.

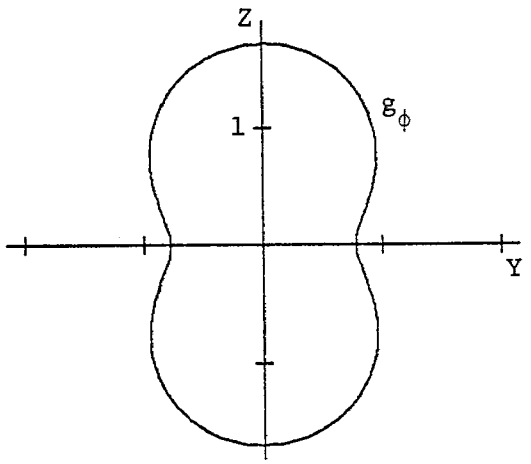

(a) G/Q = 0.573

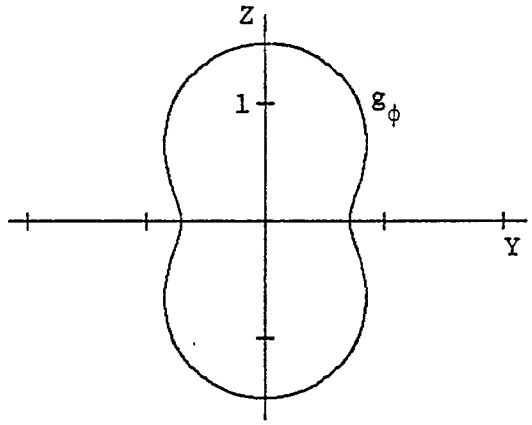

(b) G/Q = 0.566

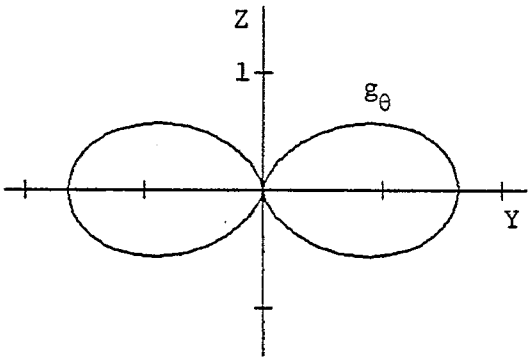

(c) G/Q = 0.198

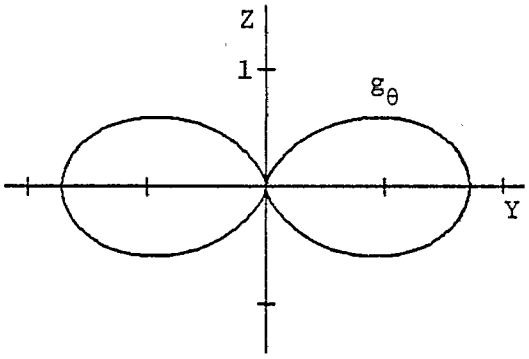

(d) G/Q = 0.106

Fig. 16. Gain patterns for the maximum G/Q currents of Fig. 14 in the x=0 plane. Field of (a) and (b) is ϕ polarized, that of (c) and (d) is θ polarized.

VI. PATTERN SYNTHESIS

The scattering pattern of a reactively loaded body can be made nearly equal to the radiation pattern of any real current, or, more generally, any equiphase current, by the resonating procedure of Section III. We now consider a synthesis method for finding a real current whose radiation pattern at M points approximates in a least-squares sense some desired pattern. Because the radiation pattern of a real current is point symmetric, the desired pattern should also be point symmetric. Furthermore, to reduce supergain effects, the source will be limited to modes having small eigenvalues.

Given a desired field pattern $\vec{E}_o$, it is desired to obtain an equiphase current $\vec{J}$ whose radiation pattern approximates $\vec{E}_o$. We assume that $\vec{J}$ is a superposition of N mode currents $\vec{J}_n$ of the form

$$\vec{J} = e^{j\beta} \sum_{n=1}^{N} \alpha_n \vec{J}_n \tag{34}$$

where the real constants α_n and β are to be determined. The radiation field of this current is

$$\vec{E} = e^{j\beta} \sum_{n=1}^{N} \alpha_n \vec{E}_n \tag{35}$$

where the $\vec{E}_n$ are characteristic fields. We set $\vec{E} = \vec{E}_o$, real and imaginary parts, at M points on the radiation sphere. If $M > N/2$, where N is the number of modes used, there are more equations than unknowns α_n to be found. In this case we can minimize the mean square error

$$\varepsilon = \sum_{m=1}^{M} \left| e^{j\beta} \sum_{n=1}^{N} \alpha_n E_n^m - E_o^m \right|^2 \tag{36}$$

where the superscripts m denote evaluation at the m-th point on the radiation sphere. In matrix notation, (36) can be written as

$$\varepsilon = \overbrace{[e^{j\beta}A\alpha - E]^*}[e^{j\beta}A\alpha - E] \tag{37}$$

where $[\alpha]$ and $[E]$ are column matrices of the α_n and E_o^m, and $[A]$ is an M by N matrix with elements

$$A_{mn} = E_n^m \tag{38}$$

The variation of ε when $[\alpha]$ is varied is

$$\delta\varepsilon = 2[\widetilde{\delta\alpha}][\mathrm{Re}(\widetilde{A}^*A)\alpha - \mathrm{Re}(e^{-j\beta}\widetilde{A}^*E)] \tag{39}$$

For $\delta\varepsilon$ to be zero for arbitrary $[\delta\alpha]$, the final bracketed term must be zero, or

$$[\alpha] = [\mathrm{Re}(\widetilde{A}^*A)]^{-1}[\mathrm{Re}(e^{-j\beta}\widetilde{A}^*E)] \tag{40}$$

Substituting this into (37), and simplifying, we have the mean square error given by

$$\varepsilon = -\mathrm{Re}[e^{-j\beta}\widetilde{\alpha}\widetilde{A}^*E] + [\widetilde{E}^*][E] \tag{41}$$

For a fixed phase β, the expansion coefficients α_n are found from (40) and the squared error from (41).

We can still adjust β to obtain the minimum ε. To do this, substitute (40) into (41) and rearrange, obtaining

$$\varepsilon = c_1\cos^2\beta + c_2\sin^2\beta + c_3\sin\beta\cos\beta + [\widetilde{E}^*][E] \tag{42}$$

where

$$c_1 = -\widetilde{[\mathrm{Re}(\widetilde{A}^*E)]}[\mathrm{Re}(\widetilde{A}^*A)]^{-1}\mathrm{Re}[\widetilde{A}^*E] \tag{43}$$

$$c_2 = -\widetilde{[\mathrm{Im}(\widetilde{A}^*E)]}[\mathrm{Re}(\widetilde{A}^*A)]^{-1}\mathrm{Im}[\widetilde{A}^*E] \tag{44}$$

$$c_3 = -2\widetilde{[\mathrm{Im}(\widetilde{A}^*E)]}[\mathrm{Re}(\widetilde{A}^*A)]^{-1}\mathrm{Re}[\widetilde{A}^*E] \tag{45}$$

Setting $\partial\varepsilon/\partial\beta = 0$, we obtain from (42)

$$\beta = \frac{1}{2}\tan^{-1}\left(\frac{c_3}{c_1 - c_2}\right) \tag{46}$$

We need consider only $-\pi/2 \leq \beta < \pi/2$, since adding π to β merely changes the sign of $\vec{J}$, as is evident from (34). There are two solutions to (46) in this range, one of which corresponds to the best choice of β and the

other the worst choice. The equiphase current for our synthesis procedure is now given by (34), where the α_n are found from (40) and β is chosen to give the smaller ε according to (41).

To test the pattern synthesis procedure, we first chose $\vec{E}_o$ to be the field radiated by the current for maximum G/Q, axial direction, for the wire triangle. This case was considered in Section V, the solution being graphed in Figs. 14a, 15a, and 16a. We set $E_\theta = (E_\theta)_o$ at 15 points in the y=0 plane, $x > 0$, and the synthesis method converged upon the current of Fig. 14a using 3 modes. (This means that the maximum G/Q current consists of three modes of the unloaded triangle.) The gain patterns were, of course, the same as those of Figs. 15a and 16a.

To illustrate the method for an arbitrarily chosen pattern, let

$$(E_\theta)_o = \cos 2(\theta - 45°) \tag{48}$$

in the y=0 plane, which is a four-lobed pattern in this plane. We set $E_\theta = (E_\theta)_o$ at 15 points in the y=0 plane, $x > 0$, and ran the synthesis program. Figure 17 shows the convergence of E_θ (solid line) to $(E_\theta)_o$ (shown by x's) as the number of modes of the unloaded triangle (Fig. 2) is increased. The first two modes contribute little to E_θ, hence we show only the cases 3, 4, 5, and 6 modes in Fig. 17. The sixth mode has $\lambda = -3930$. Hence, we would expect the synthesized pattern to be high Q, that is, frequency sensitive. Figure 18 shows the convergence of the synthesized current for the corresponding 3, 4, 5, and 6 mode cases. As modes are added, the current becomes more and more oscillatory, a property which continues as even more modes are included. This is characteristic of supergain behavior. Finally, once the equiphase current is found, we multiply it by $e^{-j\beta}$ to make it real, and then resonate it according to the procedure of Section III. This has been done for the currents of Fig. 18, and the resultant plots of σ/λ^2 are shown in Fig. 19. The incident wave was taken at the angle $\theta = 45°$ to insure that the dominant mode excitation coefficient is large. Note that the σ/λ^2 patterns correspond more or less to the synthesized patterns of Fig. 17, with the greatest distortion occurring in the 3 mode case.

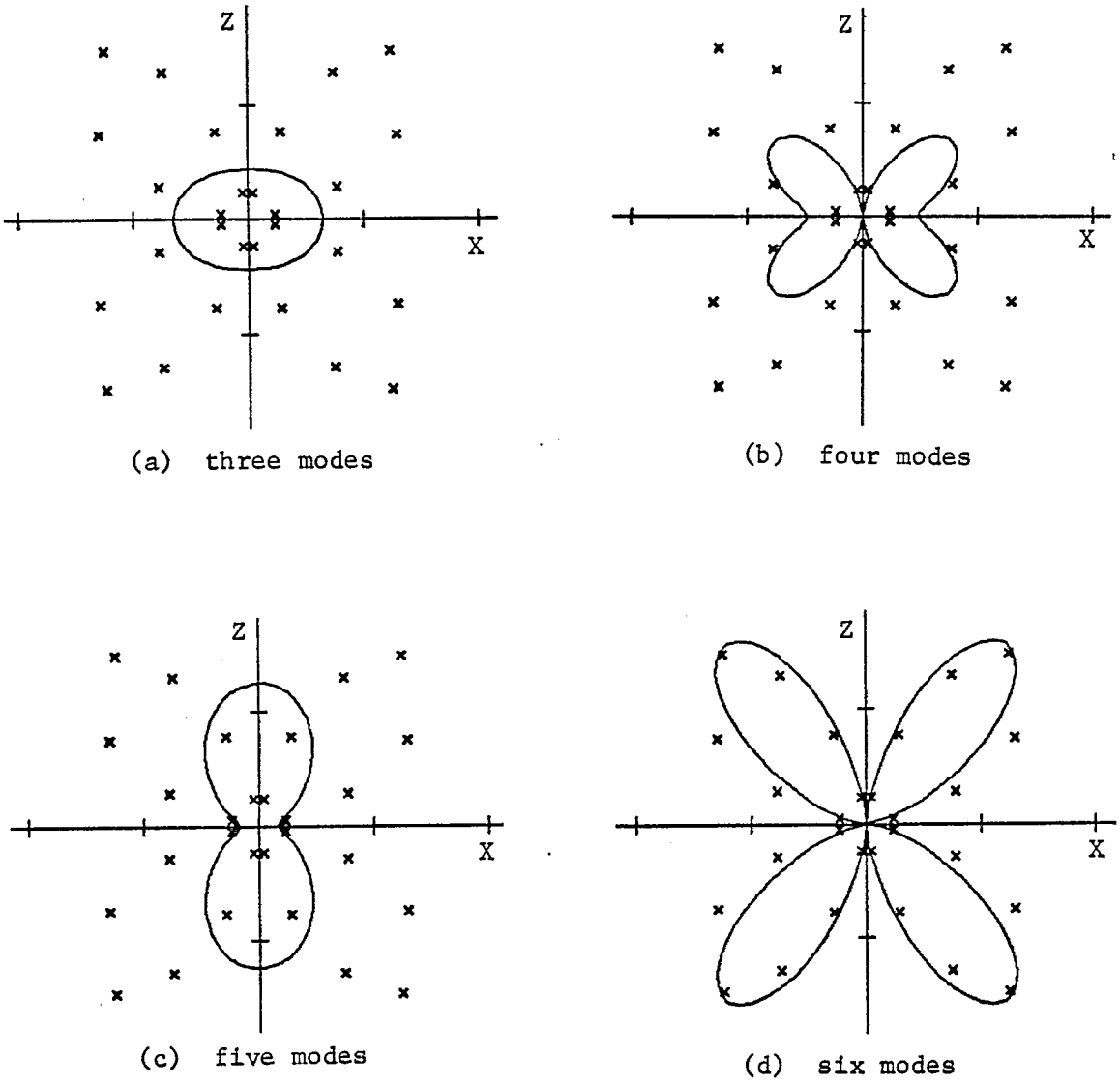

Fig. 17. Pattern synthesis of $g_\theta = E_\theta^2$ in the y=0 plane as modes are added in the order of increasing $|\lambda_n|$. Body is the wire triangle of Fig. 1. Desired g_θ is shown by x's, synthesized g_θ is shown solid.

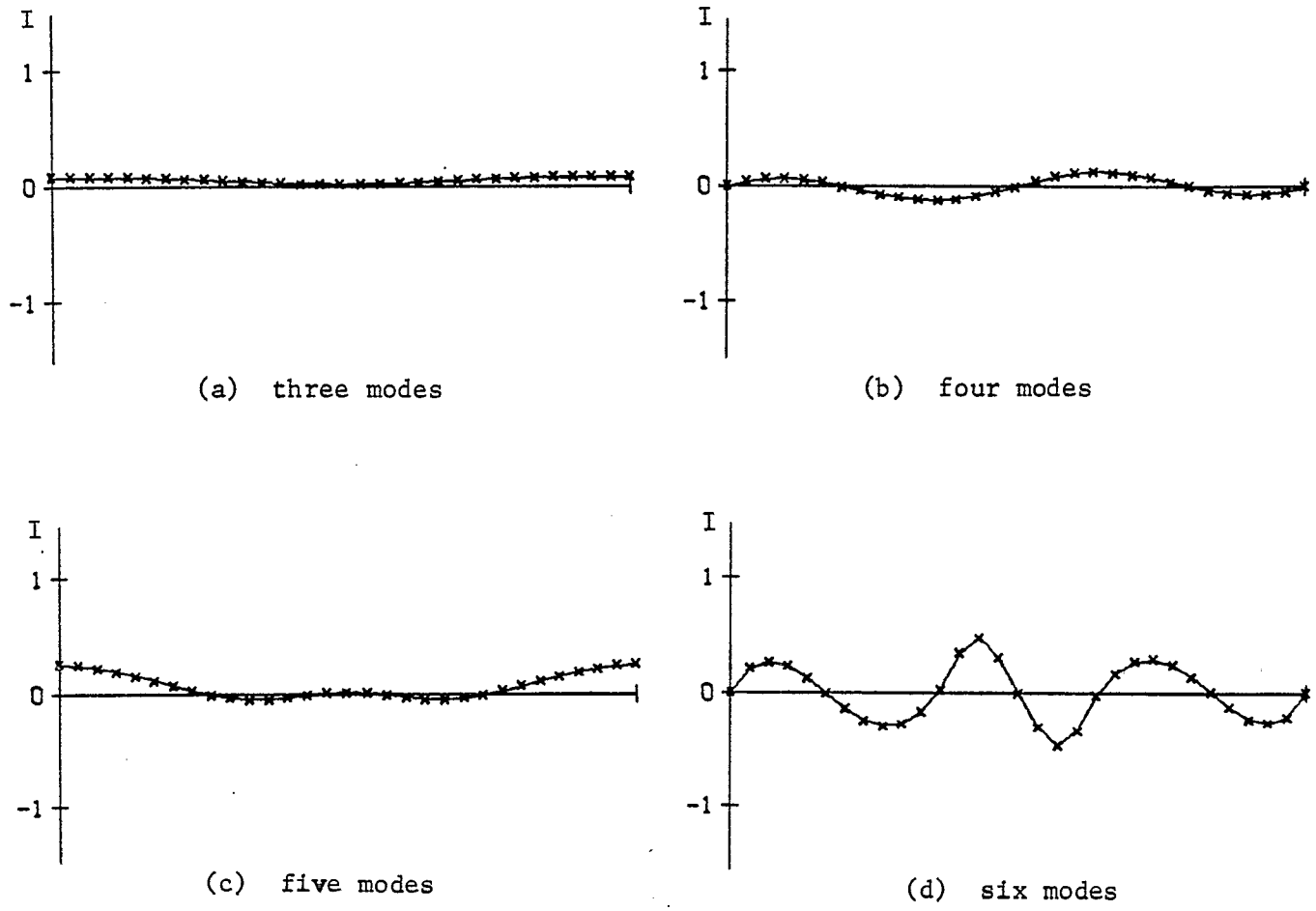

Fig. 18. Currents on the wire triangle for the synthesized patterns of Fig.17. Current continues to get more oscillatory as modes are added.

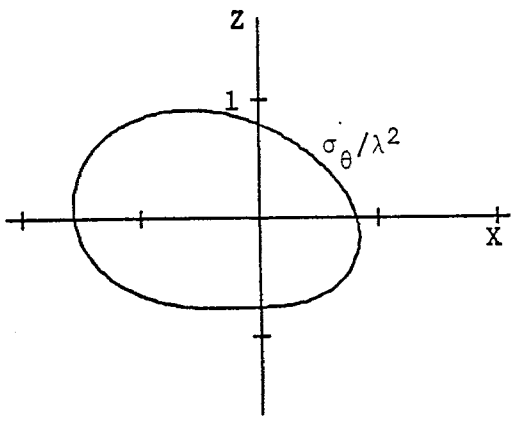

(a) 3 mode synthesis

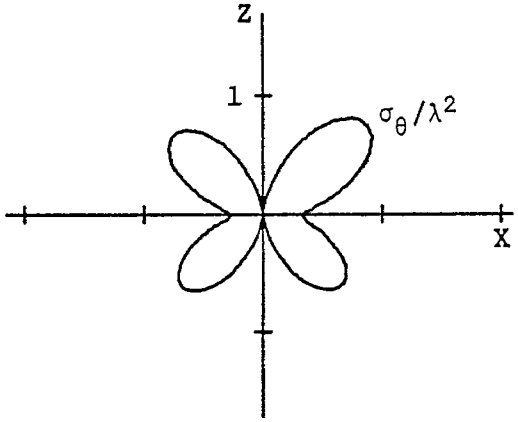

(b) 4 mode synthesis

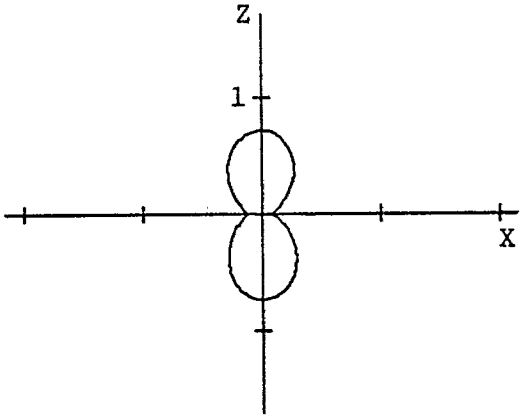

(c) 5 mode synthesis

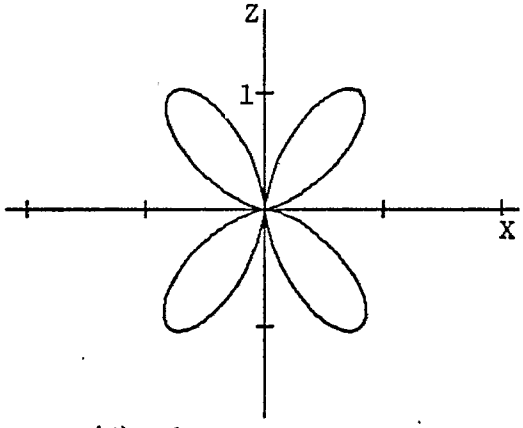

(d) 6 mode synthesis

Fig. 19. Scattering patterns for the currents of Fig. 18 (a) to (d) resonated by reactive loads on the wire triangle. Excitation is by plane wave incident at the angle $\theta = 45°$ in the y=0 plane.

VII. SPARSELY LOADED SCATTERERS

So far all examples have been for continuous loading, or, more precisely, one load per expansion function. It is suspected that, for most purposes, a few lumped loads may do almost as well as continuous loading. Scatterers with just a few loads will be called sparsely loaded scatterers. A method for resonating currents on sparsely loaded scatterers is given here to test this hypothesis.

Let the current matrix for a scatterer be partitioned as

$$[I] = \begin{bmatrix} [I]_1 \\ [I]_2 \end{bmatrix} \tag{49}$$

where $[I_1]$ is the current matrix for loaded ports, and $[I_2]$ is the current matrix for unloaded ports. The reactance matrix for the scatterer is partitioned conformably with [I], so that, in matrix form, (19) can be written as

$$\begin{bmatrix} [X_L] & [0] \\ [0] & [0] \end{bmatrix} \begin{bmatrix} [I]_1 \\ [I]_2 \end{bmatrix} = - \begin{bmatrix} [X]_{11} & [X]_{12} \\ [X]_{21} & [X]_{22} \end{bmatrix} \begin{bmatrix} [I]_1 \\ [I]_2 \end{bmatrix} \tag{50}$$

Here $[X_L]$is the load matrix for the loaded ports only. Equation (50) is a pair of simultaneous matrix equations. From the second equation, we have

$$[I]_2 = - [X]_{22}^{-1}[X]_{21}[I]_1 \tag{51}$$

Substituting this into the first matrix equation and rearranging, we obtain

$$[X_L][I]_1 = - [X_{11} - X_{12}\, X_{22}^{-1}\, X_{21}][I]_1 \tag{52}$$

If $[I]_1$ is a desired current, the loads X_{Li} to resonate it can be computed from (52).

To illustrate the behavior of sparsely loaded scatterers, the lowest Q end-fire current, Fig. 8b, of the wire triangle is chosen as the desired current. This current is first resonated with loads on every expansion function (30 loads), then loads on every other expansion function (15 loads), then 8

loads, and finally 4 loads. The resultant currents are shown in Fig. 20. In Fig. 20, (a) is the same as Fig. 8b, and the currents in the sparsely loaded cases, (b) to (d), have currents equal to those of (a) at the loaded points. At the unloaded points, the current differs from that of (a), the difference becoming greater as the number of loads is decreased. The bistatic radar cross section patterns for the four cases are shown in Fig. 21. These are plots of σ/λ^2 in the two principal planes for an axially incident plane wave. Figure 21a is the same as Fig. 11. Note that Figs. 21b and 21c are quite close to the continuously loaded case, 21a, while 21d departs considerably from it but is still a desirable radar scattering pattern.

VIII. DISCUSSION

For a given body, any real current can be resonated by reactive loads to make it the dominant mode current of that body. This real current may be chosen to optimize various parameters, such as quality factor and gain, or to synthesize a desired scattering pattern. The numerical examples included are for loaded wire objects, although similar computations have been made for conducting bodies of revolution. On wires, loads can be physically realized by lumped network elements, such as resistors, inductors, and capacitors. On bodies of revolution loads are more difficult to interpret and realize. For example, reactive loads might be approximated by tuned slots or stubs on a conducting body, but the numerical value of their equivalent reactance is not easily obtained.

Preliminary results for sparsely loaded bodies indicate that they have great potential for reactive control of radiation and scattering patterns. The approach used here was to constrain the total current to be a desired current at N ports on the body. A better approach would be to formulate the entire problem in terms of N-port parameters [5,21]. A theory using the N-port network parameters for problems of optimization and synthesis problems should in many respects parallel the theory developed in this report using generalized impedance matrices. Work along these lines is now in progress.

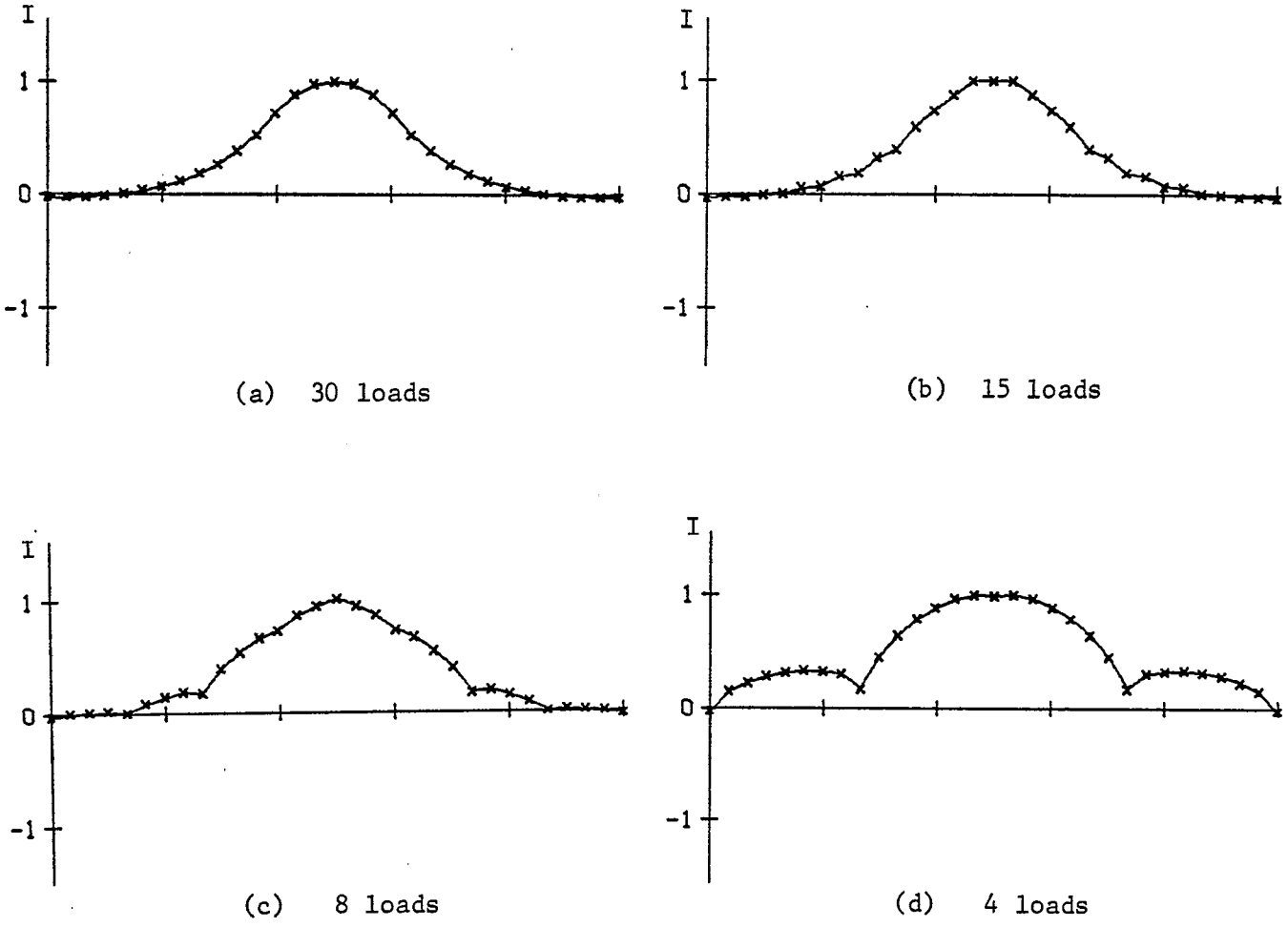

Fig. 20. Currents on the reactively loaded wire triangle as the number of loads is decreased. The resonated current at the load ports is the lowest Q end-fire current. Excitation is by a plane wave axially incident on the 30° angle.

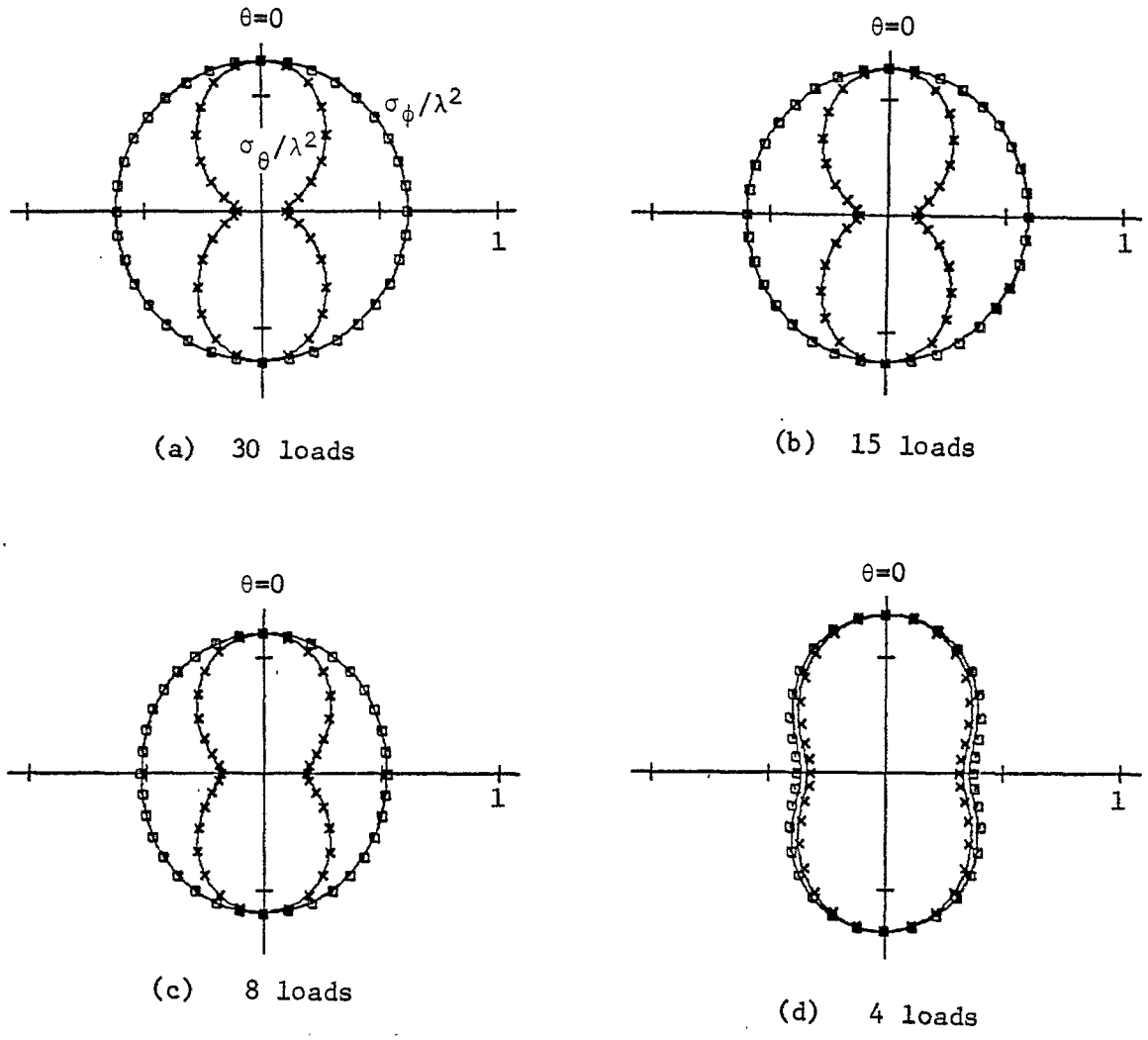

Fig. 21. Bistatic σ/λ^2 for the reactively loaded wire triangle for the currents of Fig. 20. Excitation is by a plane wave axially incident on the 30° triangle. Single mode solutions are shown by squares in the x=0 plane and by x's in the y=0 plane. Matrix inversion solutions are shown solid.

APPENDIX

OPTIMIZATION OF A RAYLEIGH QUOTIENT WHEN THE VECTOR IS REAL

For conciseness, no special notation will be used to denote vectors and matrices. In general, a Rayleigh quotient is defined as

$$\rho = \frac{\tilde{I}^* A I}{\tilde{I}^* B I} = \frac{N}{D} \tag{A-1}$$

where I is a column vector, and A and B are Hermitian matrices. If I is over the complex field the stationary points of (A-1) are the eigenvalues ρ of

$$AI = \rho\, BI \tag{A-2}$$

It is desired to determine the stationary points of (A-1) when I is over the real field. For this, we drop the conjugation on I^* and set the variation of (A-1) with respect to I equal to zero.

$$\delta\rho = \frac{1}{D^2}\left[D(\widetilde{\delta I} A I + \tilde{I} A \delta I) - N(\widetilde{\delta I} B I + \tilde{I} B \delta I)\right]$$

$$= \frac{1}{D}\,\widetilde{\delta I}\left[(A + \tilde{A})I - \rho(B + \tilde{B})I\right] = 0 \tag{A-3}$$

Since A is Hermitian, the matrix

$$\frac{1}{2}(A + \tilde{A}) = \mathrm{Re}A \tag{A-4}$$

is a real symmetric matrix with elements equal to the real parts of those of A, and similary for B. For (A-3) to hold for arbitrary δI, the term in the brackets must be zero, or

$$(\mathrm{Re}A)I = \rho(\mathrm{Re}B)I \tag{A-5}$$

Hence, for I real, the eigenvalue equation (A-5) replaces (A-2) for determining the stationary points of ρ.

For our problem, the matrix A is the one-term dyad

$$A = V^* \tilde{V} \tag{A-6}$$

where V is a complex column matrix. Let V be expressed in terms of real and imaginary parts as

$$V = V_1 + jV_2 \tag{A-7}$$

Then, substituting (A-6) into (A-4), we have

$$\mathrm{ReA} = V_1\tilde{V}_1 + V_2\tilde{V}_2 \tag{A-8}$$

This shows that ReA is a two-term dyad if V_1 and V_2 are linearly independent. Hence, all eigenvalues of (A-5) are zero except two. To find the non-zero eigenvalues, substitute (A-8) into (A-5) and obtain

$$\rho(\mathrm{ReB})I = (\tilde{V}_1 I)V_1 + (\tilde{V}_2 I)V_2 \tag{A-9}$$

Premultiplying by $(\mathrm{ReB})^{-1}$ shows that I is a linear combination of

$$I_1 = (\mathrm{ReB})^{-1}V_1 \tag{A-10}$$

and

$$I_2 = (\mathrm{ReB})^{-1}V_2 \tag{A-11}$$

Since a constant times an eigenvector is still an eigenvector, we can rewrite this linear combination as

$$I = I_1 + c\, I_2 \tag{A-12}$$

where

$$c = \tilde{V}_2 I / \tilde{V}_1 I \tag{A-13}$$

Next substitute (A-10) through (A-12) into the left-hand side of (A-9), substitute (A-12) into the right-hand side, and equate coefficients of V_1 and V_2 (assumed independent). The result is

$$\rho = \tilde{V}_1(I_1 + c\, I_2) \tag{A-14}$$

and

$$\rho = \tilde{V}_2\left(\frac{1}{c} I_1 + I_2\right) \tag{A-15}$$

These two expressions for ρ must be equal, which results in the quadratic for c

$$\tilde{V}_1 I_2 c^2 + (\tilde{V}_1 I_1 - \tilde{V}_2 I_2)c - \tilde{V}_2 I_1 = 0 \qquad \text{(A-16)}$$

From (A-10) and (A-11) it is evident that

$$\tilde{V}_1 I_2 = \tilde{V}_2 I_1 \qquad \text{(A-17)}$$

With this relationship, the two roots of (A-16) are

$$c = -a \pm \sqrt{a^2 + 1} \qquad \text{(A-18)}$$

where

$$a = \frac{\tilde{V}_1 I_1 - \tilde{V}_2 I_2}{2\tilde{V}_1 I_2} \qquad \text{(A-19)}$$

Equation (A-18) determines two real values of c, from which the stationary values of ρ are determined by (A-14) or (A-15), and the extremizing vectors by (A-12). The maximum ρ is the larger of the two stationary values.

The question arises as to how much ρ is decreased by restricting I to be real. In the text we are interested only in real positive definite matrices B, in which case ReB = B. The maximum ρ for I complex is then

$$\rho_{com.} = \tilde{V} B^{-1} V^*$$

$$= \tilde{V}_1 B^{-1} V_1 + \tilde{V}_2 B^{-1} V_2 \qquad \text{(A-20)}$$

The maximum ρ for I real is given by (A-14). Substituting for c from (A-18) into (A-14), simplifying, and taking the larger value, we have

$$\rho_{real} = \frac{1}{2}\rho_{com.} + \left|\sqrt{a^2 + 1}\,\tilde{V}_1 I_2\right| \qquad \text{(A-21)}$$

From this it is evident that the maximum ρ's are related by

$$\frac{1}{2}\rho_{com.} \leq \rho_{real} \leq \rho_{com.} \qquad \text{(A-22)}$$

The left-hand equality is attained when V_1 and I_2 are orthogonal, that is, when $\tilde{V}_1 I_2 = 0$. The right-hand equality is attained when V is of constant phase, that is, when $V_2 = bV_1$ where b is any real constant.

PART TWO

PROGRAM DESCRIPTIONS AND LISTINGS

I. INTRODUCTION

The programs used to compute the examples of part one, except those appearing in previous reports, are described and listed here in part two. Each program is accompanied by operating instructions and sample input-output data. To facilitate reference to the theory, this part of the report is divided into sections having the same headings as the corresponding sections of part one.

II. MODES OF A LOADED SURFACE

The computer programs of Sections III, IV, and V of reference [20] are written for use on both unloaded and loaded bodies. It is merely necessary to read in the proper load matrix $[Z_L]$ to be added to [Z]. These programs calculate the mode currents, the mode gain patterns, and the modal solution for bistatic radar cross section.

III. RESONATING A DESIRED REAL CURRENT

This program calculates the loads which make a given real current a mode current of the loaded surface with eigenvalue zero. The activity on data sets 1 (punched card input), 2 (punched card output), and 6 (direct access input-output) is as follows.

```
      READ(1,10) N, MD5, N6
10    FORMAT(20I3)
      REWIND 6
      NZ = N*N
      SKIP N6 RECORDS ON DATA SET 6
      READ(6) (Z(I), I = 1, NZ)
      DO 16 J = 1, MD5
      READ(1,28) (FI(I), I = 1, N)
```

```
28    FORMAT(10F8.4)
      WRITE(2,26) (XL(I), I = 1, N)
26    FORMAT(7E11.4)
16    CONTINUE
```

The program in Section II of [20] has already calculated and stored the impedance matrix Z of order N on the $(N6+1)^{th}$ record of data set 6. The program in Section II of [20] gives an unsymmetric impedance matrix Z, but all the programs of the present report require a symmetric impedance matrix Z. The addition of the statements

```
      DO 41 J = 1, N
      J1 = (J-1)*N
      DO 42 I = 1,J
      J2 = J1 + I
      J3 = (I-1)*N + J
      Z(J2) = .5*(Z(J2) + Z(J3))
      Z(J3) = Z(J2)
42    CONTINUE
41    CONTINUE
```

just after the CALL CALZ statement in the main program in Section II of [20] will make the impedance matrix Z symmetric by averaging corresponding off diagonal elements. The load reactances XL are computed from the currents FI in DO loop 16 according to (19).

Minimum allocations are given by

```
      COMPLEX Z(N*N)
      DIMENSION X(N*N), FI(N), XL(N)
```

The sample data and printed output are taken to resonate the $\lambda = 31.84$ mode of the unloaded wire triangle of Fig. 1. Note that the program of Section III of [20] writes the mode currents on direct access data set 6 instead of punching them out.

The mode currents, the mode gain patterns, and the modal solution of bistatic radar cross section are computed by the programs in sections III, IV, and V of [20]. Note also that the programs of [20] are more general in

that they will admit complex loads ZL instead of reactive loads XL. The user must either modify the programs of [20] to accept the real XL instead of the complex ZL or modify the program of Section III to punch out XL interspersed with zeros to represent zero resistive loads.

LISTING OF PROGRAM TO CALCULATE REACTIVE LOADS TO RESONATE A DESIRED REAL CURRENT

```
//              (0034,EE,2,2,5),'MAUTZ,JOE',REGION=140K
// EXEC FORTGCLG,PARM.FORT='MAP'
//FORT.SYSIN DD *
      COMPLEX Z(900)
      DIMENSION X(900),FI(30),XL(30)
      READ(1,10) N,MD5,N6
   10 FORMAT(20I3)
      WRITE(3,11) N,MD5,N6
   11 FORMAT('0 N MD5 N6'/1X,3I3)
      REWIND 6
      NZ=N*N
      IF(N6) 13,13,14
   14 DO 15 J=1,N6
      READ(6)
   15 CONTINUE
   13 READ(6)(Z(I),I=1,NZ)
      WRITE(3,27)(Z(I),I=1,3)
   27 FORMAT('0Z'/(1X,10E11.4))
      DO 22 I=1,NZ
      X(I)=AIMAG(Z(I))
   22 CONTINUE
      DO 16 J=1,MD5
      READ(1,28)(FI(I),I=1,N)
   28 FORMAT(10F8.4)
      WRITE(3,29)(FI(I),I=1,N)
   29 FORMAT('0FI'/(1X,10F8.4))
      DO 23 I=1,N
      J1=(I-1)*N
      S1=0.
      DO 24 K=1,N
      J2=J1+K
      S1=S1+X(J2)*FI(K)
   24 CONTINUE
      XL(I)=-S1/FI(I)
   23 CONTINUE
      WRITE(3,25)(XL(I),I=1,N)
   25 FORMAT('0XL'/(1X,7E11.4))
      WRITE(2,26)(XL(I),I=1,N)
   26 FORMAT(7E11.4)
   16 CONTINUE
      STOP
      END
```

```
/*
//GO.FT06F001 DD DSNAME=EE0034.REV1,DISP=OLD,UNIT=2314,                X
//              VOLUME=SER=SU0004,DCB=(RECFM=VS,BLKSIZE=2596,LRECL=2592)
//GO.SYSIN DD *
 30   1   0
  0.9240   0.9463   0.9678   0.9849   0.9959   1.0000   0.9969   0.9866   0.9695   0.9464
  0.9184   0.8871   0.8567   0.8453   0.8408   0.8394   0.8408   0.8453   0.8567   0.8871
  0.9184   0.9464   0.9695   0.9866   0.9969   1.0000   0.9959   0.9849   0.9678   0.9463
/*
//
```

SAMPLE PRINTED OUTPUT

```
 N MD5 N6
 30   1   0
```

```
/
 0.5801E-01-0.5873E+03 0.5810E-01 0.2657E+03 0.5784E-01 0.3124E+02

FI
  0.9240   0.9463   0.9678   0.9849   0.9959   1.0000   0.9969   0.9866   0.9695   0.9464
  0.9184   0.8871   0.8567   0.8453   0.8408   0.8394   0.8408   0.8453   0.8567   0.8871
  0.9184   0.9464   0.9695   0.9866   0.9969   1.0000   0.9959   0.9849   0.9678   0.9463

XL
-0.3283E+02-0.3349E+02-0.3509E+02-0.3650E+02-0.3786E+02-0.3918E+02-0.4043E+02
-0.4171E+02-0.4300E+02-0.4419E+02-0.4521E+02-0.4618E+02-0.5183E+02-0.5777E+02
-0.5903E+02-0.5948E+02-0.5903E+02-0.5777E+02-0.5183E+02-0.4618E+02-0.4521E+02
-0.4419E+02-0.4300E+02-0.4171E+02-0.4043E+02-0.3918E+02-0.3786E+02-0.3650E+02
-0.3509E+02-0.3349E+02
```

IV. BROADBAND SCATTERERS

The eigenvalues Q and eigenvectors [I] of (24) can be computed by the program in Section III of [20] if [R] + j[ωX'] is stored in place of [Z].

A program to store [R] + j[ωX'] on data set 6 is described next. The activity on data sets 1 (punched card input) and 6 (direct access input-output) is as follows.

```
      REWIND 6
      READ(1,7) N4
7     FORMAT(20I3)
      DO 15 L = 1, N4
      READ(1,8) N, N5, N6, N7, D
8     FORMAT(4I3, E11.4)
      NZ = N*N
      SKIP N5 RECORDS ON DATA SET 6
      READ(6) (Z1(I), I = 1, NZ)
      SKIP N6 RECORDS ON DATA SET 6
      READ(6)(Z2(I), I = 1, NZ)
      SKIP N7 RECORDS ON DATA SET 6
      WRITE(6) (Z(I), I = 1, NZ)
15    CONTINUE
```

The impedance matrices at propagation constants k and k(1.+D) have been stored on the (N5+1)th and (N5+N6+2)th records of data set 6 by the program of Section II of [20] with the modification given in Section III of the present report. [R] + j[ωX'] is stored in Z and written on the (N5+N6+N7+3)th record of data set 6. A finite difference approximation is used in DO loop 12 to calculate [X']. Minimum allocations are given by

```
      COMPLEX Z1(N*N), Z2(N*N), Z(N*N)
```

The sample input data and printed output are for the wire triangle of Fig. 1.

LISTING OF PROGRAM TO STORE R+JWX' ON DATA SET 6

```
//              (0034,EE,2,2),'MAUTZ,JOE',REGION=140K
// EXEC FORTGCLG,PARM.FORT='MAP'
//FORT.SYSIN DD *
      COMPLEX Z1(900),Z2(900),Z(900),U
      REWIND 6
      READ(1,7) N4
    7 FORMAT(20I3)
      WRITE(3,10) N4
   10 FORMAT('0N4'/(1X,I3))
      DO 15 L=1,N4
      READ(1,8) N,N5,N6,N7,D
    8 FORMAT(4I3,E11.4)
      WRITE(3,9) N,N5,N6,N7,D
    9 FORMAT('0 N  N5 N6 N7',5X,'D'/1X,4I3,E11.4)
      NZ=N*N
      J1=IABS(N5)
      IF(N5) 16,17,18
   16 DO 19 J=1,J1
      BACKSPACE 6
   19 CONTINUE
      GO TO 17
   18 DO 20 J=1,J1
      READ(6)
   20 CONTINUE
   17 READ(6)(Z1(I),I=1,NZ)
      WRITE(3,11)(Z1(I),I=1,3)
   11 FORMAT('0Z1'/(1X,10E11.4))
      J1=IABS(N6)
      IF(N6) 21,22,23
   21 DO 24 J=1,J1
      BACKSPACE 6
   24 CONTINUE
      GO TO 22
   23 DO 25 J=1,J1
      READ(6)
   25 CONTINUE
   22 READ(6)(Z2(I),I=1,NZ)
      WRITE(3,13)(Z2(I),I=1,3)
   13 FORMAT('0Z2'/(1X,10E11.4))
      U=(0.,1.)/D
      DO 12 J=1,NZ
      Z(J)=REAL(Z1(J))+U*AIMAG(Z2(J)-Z1(J))
   12 CONTINUE
      WRITE(3,26)(Z(I),I=1,3)
   26 FORMAT('0Z'/(1X,10E11.4))
      J1=IABS(N7)
      IF(N7) 27,28,29
   27 DO 30 J=1,J1
      BACKSPACE 6
   30 CONTINUE
      GO TO 28
   29 DO 31 J=1,J1
      READ(6)
   31 CONTINUE
   28 WRITE(6)(Z(I),I=1,NZ)
   15 CONTINUE
      STOP
      END
```

```
/*
//GO.FT06F001 DD DSNAME=EE0034.REV1,DISP=OLD,UNIT=2314,                    X
//              VOLUME=SER=SU0004,DCB=(RECFM=VS,BLKSIZE=2596,LRECL=2596)
//GO.SYSIN DD *
  1
 30   0   0   0 0.1000E-02
/*
//
```

SAMPLE PRINTED OUTPUT

```
N4
  1

 N   N5  N6  N7      D
 30   0   0   0 0.1000E-02

Z1
 0.5801E-01-0.5873E+03 0.5810E-01 0.2657E+03 0.5784E-01 0.3124E+02

Z2
 0.5811E-01-0.5867E+03 0.5822E-01 0.2655E+03 0.5796E-01 0.3121E+02

Z
 0.5801E-01 0.5994E+03 0.5810E-01-0.2583E+03 0.5784E-01-0.3020E+02
```

Programs to calculate backscattering cross section versus frequency and to calculate patterns of σ/λ^2 from the matrix inversion solution are not included because they are essentially bits and pieces of the program in Section IV of [20]. Instead of modifying the program in Section IV of [20] it may be easier for the user to base his pattern programs on the program included in the present section which calculates the receiver excitations VR. An element of VR is the reaction between a unit incident plane wave and one of the functions used to expand the electric current.

The receiver excitations VR are calculated by the subroutine VOLT which requires some common data from the main program. The punched card input to the main program is as follows.

```
      READ(1,9) NP, NW, BK, THET
9     FORMAT(2I3, 2E14.7)
      READ(1,10)(PX(I), I = 1, NP)
      READ(1,10)(PY(I), I = 1, NP)
      READ(1,10)(PZ(I), I = 1, NP)
10    FORMAT(10F8.4)
      READ(1,15)(LL(I), I = 1, NW)
15    FORMAT(20I3)
```

The PX, PY, and PZ are the x,y, and z coordinates of NP data points describing the axes of NW wires. There is an odd number greater than or equal to 5 of data points on each wire. The data points must be arranged so that there are n-1 linearly independent triangular expansion functions peaked at a junction with n branches. BK is the propagation constant k. The receiver excitations VR will be computed for the six different incident unit plane waves $\vec{E}^r$ given by (17)-(22) of [20]. THET is either θ in (17)-(20) of [20] or ϕ in (21)-(22) of [20]. The LL(J)th data point marks the beginning of the Jth wire.

In DO loop 8, TX, TY, and TZ are $\vec{u}_\ell \cdot \vec{u}_x$, $\vec{u}_\ell \cdot \vec{u}_y$, and $\vec{u}_\ell \cdot \vec{u}_z$ while BX, BY, and BZ are kx', ky', and kz' evaluated midway between the Jth and (J-1)th data points. AL(N1) is the distance between the Jth and (J-1)th data points. DO loop 8 reckons that there will be N=J4-2 triangular expansion functions, the L(J)th being the first one on the Jth wire.

The domain of each triangular expansion function is broken up into four not necessarily equal segments, two on the upward sloping side and two on the downward sloping side. The T((J-1)*4+K) calculated for K=1,2,3,4 by DO loop 5 is the integral of the Jth triangular expansion function over its Kth segment.

The subroutine VOLT stores

$$\int_{\substack{\text{wire}\\ \text{axis}}} \vec{E}^r(\ell') \cdot u_{\ell'} T_I(\ell') d\ell' = \sum_{K=1}^{4} [\vec{E}^r(\ell') \cdot \vec{u}_{\ell'}]_K \int_{\text{Kth segment}} T_I(\ell') d\ell' \quad (53)$$

in VR((J-1)*N+I) where $[\vec{E}^r(\ell') \cdot \vec{u}_{\ell'}]_K$ is the Jth of the set (17)-(22) of [20] evaluated at the center of the Kth segment of the Ith triangular expansion function $T_I(\ell')$. In DO loop 30, the six variables ZZ(I), ZZ(J2), ZZ(J3), ZZ(J4), ZZ(J5), and ZZ(J6) correspond to the six equations of the set (17)-(22) of [20]. The number $[\vec{E}^r(\ell') \cdot \vec{u}_{\ell'}]_K$ of (17) of [20] for the Ith triangular function is stored in

```
ZZ((I-1)*2 + (M-1)* 2 + K)
```

if the Ith triangle function is on the Mth wire. DO loop 52 performs the sum on K appearing in [20]. DO loop 53 obtains each of the six $\vec{E}^r(\ell') \cdot u_{\ell'}$ of the set (17)-(22) of [20] while DO loop 49 obtains the Ith expansion function.

Minimum allocations are given by

```
COMPLEX VR(N*6), ZZ(N1*6)
COMMON L(NW+1), T(N*4), BX(N1), BY(N1), BZ(N1),
       TX(N1), TY(N1), TZ(N1)
```

in the subroutine VOLT and by

```
COMPLEX VR(N*6), ZZ(N1*6)
COMMON L(NW+1), T(N*4), BX(N1), BY(N1), BZ(N1),
      TX(N1), TY(N1), TZ(N1)
DIMENSION PX(NP), PY(NP), PZ(NP), LL(NW+1), AL(N1)
```

in the main program where

$$N1 = NP - NW$$

$$N = N1/2 - NW$$

The sample punched card input and printed output is for the wire triangle of Fig. 1. The receiver excitations are computed for all six of the polarizations (17)-(22) of [20] with θ and ϕ equal to $\pi/4$ but only the results for the third polarization $\vec{u}_\theta$, y=0 are printed out.

LISTING OF PROGRAM TO CALCULATE RECEIVER EXCITATIONS VR

```
//              (0034,EE,2,2),'MAUTZ,JOE',REGION=140K
// EXEC FORTGCLG,PARM.FORT='MAP'
//FORT.SYSIN DD *
      SUBROUTINE VOLT
      COMPLEX VR(180),U,ZZ(372),U3,U4,U5
      COMMON VR,U,ZZ,SN,CS,N1,L(5),N,NN6
      COMMON T(120),BX(100),BY(100),BZ(100),TX(100),TY(100),TZ(100)
      DO 30 I=1,N1
      S1=-BY(I)*SN
      S2=BZ(I)*CS
      S3=S1+S2
      S4=BX(I)*SN+S2
      S5=BX(I)*CS-S1
      U3=COS(S3)+U*SIN(S3)
      U4=COS(S4)+U*SIN(S4)
      U5=COS(S5)+U*SIN(S5)
      S1=TY(I)*CS
      S2=TZ(I)*SN
      J2=I+N1
      J3=J2+N1
      J4=J3+N1
      J5=J4+N1
      J6=J5+N1
      ZZ(I)=(-S2-S1)*U3
      ZZ(J2)=TX(I)*U3
      ZZ(J3)=(TX(I)*CS-S2)*U4
      ZZ(J4)=TY(I)*U4
      ZZ(J5)=-TZ(I)*U5
      ZZ(J6)=(-TX(I)*SN+S1)*U5
   30 CONTINUE
      J4=-2
      J5=1
      DO 49 I=1,N
      J2=(I-1)*4
      IF(L(J5)-I) 50,51,50
   51 J4=J4+2
      J5=J5+1
```

```
 50 J6=J4
    DO 53 J=I,NN6,N
    VR(J)=0.
    DO 52 K=1,4
    K3=J6+K
    K2=J2+K
    VR(J)=T(K2)*ZZ(K3)+VR(J)
 52 CONTINUE
    J6=J6+N1
 53 CONTINUE
    J4=J4+2
 49 CONTINUE
    RETURN
    END
    COMPLEX VR(180),U,ZZ(372)
    COMMON VR,U,ZZ,SN,CS,N1,L(5),N,NN6
    COMMON T(120),BX(100),BY(100),BZ(100),TX(100),TY(100),TZ(100)
    DIMENSION PX(100),PY(100),PZ(100),LL(5),AL(100)
    U=(0.,1.)
    READ(1,9) NP,NW,BK,THET
  9 FORMAT(2I3,2E14.7)
    WRITE(3,14) NP,NW,BK,THET
 14 FORMAT('0 NP NW',6X,'BK',11X,'THET'/1X,2I3,2E14.7)
    READ(1,10)(PX(I),I=1,NP)
    READ(1,10)(PY(I),I=1,NP)
    READ(1,10)(PZ(I),I=1,NP)
 10 FORMAT(10F8.4)
    WRITE(3,11)(PX(I),I=1,NP)
    WRITE(3,12)(PY(I),I=1,NP)
    WRITE(3,13)(PZ(I),I=1,NP)
 11 FORMAT('0PX'/(1X,10F8.4))
 12 FORMAT('0PY'/(1X,10F8.4))
 13 FORMAT('0PZ'/(1X,10F8.4))
    READ(1,15)(LL(I),I=1,NW)
 15 FORMAT(20I3)
    WRITE(3,16)(LL(I),I=1,NW)
 16 FORMAT('0LL'/(1X,20I3))
    LL(NW+1)=200
    BK5=.5*BK
    N1=0
    J4=2
    J1=1
    DO 8 J=1,NP
    IF(LL(J1)-J) 7,6,7
  6 J4=J4-1
    L(J1)=J4
    J1=J1+1
    GO TO 8
  7 N1=N1+1
    J3=J-1
    IF((N1/2*2-N1).EQ.0) J4=J4+1
    S1=PX(J)-PX(J3)
    S2=PY(J)-PY(J3)
```

```
      S3=PZ(J)-PZ(J3)
      S4=SQRT(S1*S1+S2*S2+S3*S3)
      TX(N1)=S1/S4
      TY(N1)=S2/S4
      TZ(N1)=S3/S4
      BX(N1)=BK5*(PX(J)+PX(J3))
      BY(N1)=BK5*(PY(J)+PY(J3))
      BZ(N1)=BK5*(PZ(J)+PZ(J3))
      AL(N1)=S4
    8 CONTINUE
      N=J4-2
      L(J1)=J4
      J1=1
      J2=-2
      DO 5 J=1,N
      IF(L(J1)-J) 3,4,3
    4 J2=J2+2
      J1=J1+1
    3 J4=(J-1)*4+1
      J5=J4+1
      J6=J5+1
      J7=J6+1
      K4=J2+1
      K5=K4+1
      K6=K5+1
      K7=K6+1
      S1=AL(K4)+AL(K5)
      S2=AL(K6)+AL(K7)
      T(J4)=AL(K4)*.5*AL(K4)/S1
      T(J5)=AL(K5)*(AL(K4)+.5*AL(K5))/S1
      T(J6)=AL(K6)*(AL(K7)+.5*AL(K6))/S2
      T(J7)=AL(K7)*.5*AL(K7)/S2
      J2=J2+2
    5 CONTINUE
      SN=SIN(THET)
      CS=COS(THET)
      NN6=N*6
      CALL VOLT
      J1=2*N+1
      J2=3*N
      WRITE(3,17)(VR(J),J=J1,J2)
   17 FORMAT('OVR'/(1X,7E11.4))
      STOP
      END
/*
//GO.SYSIN DD *
 63   1 0.1039861E+00 0.7853982E+00
 -0.5176 -0.2588  0.0000  0.2588  0.5176  0.7765  1.0353  1.2941  1.5529  1.8117
  2.0706  2.3294  2.5882  2.8470  3.1058  3.3646  3.6235  3.8823  4.1411  4.3999
  4.6587  4.9176  5.1764  5.4352  5.6940  5.9528  6.2117  5.1764  4.1411  3.1058
  2.0706  1.0353  0.0000 -1.0353 -2.0706 -3.1058 -4.1411 -5.1764 -6.2117 -5.9528
 -5.6940 -5.4352 -5.1764 -4.9176 -4.6587 -4.3999 -4.1411 -3.8823 -3.6235 -3.3646
 -3.1058 -2.8470 -2.5882 -2.3294 -2.0706 -1.8117 -1.5529 -1.2941 -1.0353 -0.7765
 -0.5176 -0.2588 -0.0000
  0.0000  0.0000  0.0000  0.0000  0.0000  0.0000  0.0000  0.0000  0.0000  0.0000
  0.0000  0.0000  0.0000  0.0000  0.0000  0.0000  0.0000  0.0000  0.0000  0.0000
  0.0000  0.0000  0.0000  0.0000  0.0000  0.0000  0.0000  0.0000  0.0000  0.0000
  0.0000  0.0000  0.0000  0.0000  0.0000  0.0000  0.0000  0.0000  0.0000  0.0000
  0.0000  0.0000  0.0000  0.0000  0.0000  0.0000  0.0000  0.0000  0.0000  0.0000
  0.0000  0.0000  0.0000  0.0000  0.0000  0.0000  0.0000  0.0000  0.0000  0.0000
  0.0000  0.0000  0.0000
```

```
 1.9319   0.9659   0.0000   0.9659   1.9319   2.8978   3.8637   4.8296   5.7956   6.7615
 7.7274   8.6933   9.6593  10.6252  11.5911  12.5570  13.5230  14.4889  15.4548  16.4207
17.3867  18.3526  19.3185  20.2844  21.2504  22.2163  23.1822  23.1822  23.1822  23.1822
23.1822  23.1822  23.1822  23.1822  23.1822  23.1822  23.1822  23.1822  23.1822  22.2163
21.2504  20.2844  19.3185  18.3526  17.3867  16.4207  15.4548  14.4889  13.5230  12.5570
11.5911  10.6252   9.6593   8.6933   7.7274   6.7615   5.7956   4.8296   3.8637   2.8978
 1.9319   0.9659   0.0000
 1
/*
//
```

SAMPLE PRINTED OUTPUT

```
NP NW       BK             THET
63  1 0.1039861E+00 0.7853982E+00

PX
-0.5176 -0.2588  0.0000  0.2588  0.5176  0.7765  1.0353  1.2941  1.5529  1.8117
 2.0706  2.3294  2.5882  2.8470  3.1058  3.3646  3.6235  3.8823  4.1411  4.3999
 4.6587  4.9176  5.1764  5.4352  5.6940  5.9528  6.2117  5.1764  4.1411  3.1058
 2.0706  1.0353  0.0000 -1.0353 -2.0706 -3.1058 -4.1411 -5.1764 -6.2117 -5.9528
-5.6940 -5.4352 -5.1764 -4.9176 -4.6587 -4.3999 -4.1411 -3.8823 -3.6235 -3.3646
-3.1058 -2.8470 -2.5882 -2.3294 -2.0706 -1.8117 -1.5529 -1.2941 -1.0353 -0.7765
-0.5176 -0.2588 -0.0000

PY
 0.0000  0.0000  0.0000  0.0000  0.0000  0.0000  0.0000  0.0000  0.0000  0.0000
 0.0000  0.0000  0.0000  0.0000  0.0000  0.0000  0.0000  0.0000  0.0000  0.0000
 0.0000  0.0000  0.0000  0.0000  0.0000  0.0000  0.0000  0.0000  0.0000  0.0000
 0.0000  0.0000  0.0000  0.0000  0.0000  0.0000  0.0000  0.0000  0.0000  0.0000
 0.0000  0.0000  0.0000  0.0000  0.0000  0.0000  0.0000  0.0000  0.0000  0.0000
 0.0000  0.0000  0.0000  0.0000  0.0000  0.0000  0.0000  0.0000  0.0000  0.0000
 0.0000  0.0000  0.0000

PZ
 1.9319   0.9659   0.0000   0.9659   1.9319   2.8978   3.8637   4.8296   5.7956   6.7615
 7.7274   8.6933   9.6593  10.6252  11.5911  12.5570  13.5230  14.4889  15.4548  16.4207
17.3867  18.3526  19.3185  20.2844  21.2504  22.2163  23.1822  23.1822  23.1822  23.1822
23.1822  23.1822  23.1822  23.1822  23.1822  23.1822  23.1822  23.1822  23.1822  22.2163
21.2504  20.2844  19.3185  18.3526  17.3867  16.4207  15.4548  14.4889  13.5230  12.5570
11.5911  10.6252   9.6593   8.6933   7.7274   6.7615   5.7956   4.8296   3.8637   2.8978
 1.9319   0.9659   0.0000

LL
  1

VR
 0.3666E+00 0.3734E-04-0.9808E+00-0.1786E+00-0.9330E+00-0.3514E+00-0.8550E+00
-0.5129E+00-0.7492E+00-0.6577E+00-0.6193E+00-0.7813E+00-0.4693E+00-0.8796E+00
-0.3042E+00-0.9494E+00-0.1292E+00-0.9886E+00 0.5001E-01-0.9957E+00 0.2276E+00
-0.9706E+00 0.3978E+00-0.9142E+00 0.6216E+00-0.1063E+01 0.6200E+00-0.1323E+01
 0.4122E+00-0.1402E+01 0.1949E+00-0.1448E+01-0.2699E-01-0.1461E+01-0.2482E+00
-0.1440E+01 0.1143E+00 0.1038E+00 0.7165E+00 0.1575E+01 0.8761E+00 0.1492E+01
 0.1026E+01 0.1393E+01 0.1165E+01 0.1279E+01 0.1292E+01 0.1151E+01 0.1404E+01
 0.1011E+01 0.1502E+01 0.8596E+00 0.1583E+01 0.6991E+00 0.1647E+01 0.5311E+00
 0.1693E+01 0.3573E+00 0.1721E+01 0.1796E+00
```

V. MAXIMUM GAIN-QUALITY RATIO

The program described in this section computes both the real and complex currents (33) and (29) for maximum gain-quality ratio. The activity on data sets 1 (punched card input) and 6 (direct access input-output) is as follows.

```
      READ(1,7) N, N5, N6, BK
7     FORMAT(3I3, E14.7)
      REWIND 6
      NZ = N*N
      SKIP N6 RECORDS ON DATA SET 6
      READ(6) (Z(I), I = 1, NZ)
      DO 15 K=1, N5
      READ(1, 16)(VR(I), I = 1, N)
16    FORMAT(7E11.4)
15    CONTINUE
```

The first program described in Section IV has stored $[R] + j[\omega X']$ for propagation constant BK on the (N6+1)th record of data set 6. The complex variable VR is the receiver excitation computed by the second program described in Section IV.

It was necessary to multiply $[\omega X']$ by 0.1 in DO loop 14 to avoid an overflow in the matrix inversion subroutine MINV. [23] DO loop 19 stores the complex current (29) in FI. The gain-quality ratio attained by this complex current (29) will be stored in GB2. If either the real or imaginary part of the complex current (29) is zero, (32) becomes impossible to compute. In this case the maximum gain-quality ratio GB1 attainable by a real current is set equal to GB2, the real current for maximum gain-quality ratio is stored in CUR by DO loop 28, and execution proceeds to statement 29. If the complex current has both non-trivial real and imaginary parts, the logic between statements 27 and 29 implements (30), (31), (32), and (33). DO loop 33 normalizes CUR so that the element largest in magnitude is unity.

Minimum allocations are given by

```
COMPLEX Z(N*N), VR(N), FI(N)
DIMENSION XP(N*N), XP1(N*N), LA(N), LB(N),
     RV(N), AV(N), RI(N), AI(N), CUR(N)
```

The particular receiver excitation VR appearing in the sample input data was taken from the sample printed output of the second program in Section IV.

LISTING OF PROGRAM TO COMPUTE CURRENTS FOR MAXIMUM GAIN-QUALITY RATIO

```
//              (0034,EE,3,2),'MAUTZ,JOE',REGION=140K
// EXEC SSPCLG,PARM.FORT='MAP'
//FORT.SYSIN DD *
      COMPLEX Z(900),VR(30),FI(30)
      DIMENSION XP(900),XP1(900),LA(30),LB(30),RV(30),AV(30),RI(30)
      DIMENSION AI(30),CUR(30)
      READ(1,7) N,N5,N6,BK
    7 FORMAT(3I3,E14.7)
      WRITE(3,8) N,N5,N6,BK
    8 FORMAT('0 N  N5 N6',6X,'BK'/1X,3I3,E14.7)
      ETA=376.730
      PI=3.141593
      C1=BK*BK*ETA/(4.*PI)
      REWIND 6
      NZ=N*N
      IF(N6) 10,10,12
   12 DO 13 J=1,N6
      READ(6)
   13 CONTINUE
   10 READ(6)(Z(I),I=1,NZ)
      DO 14 J=1,NZ
      XP(J)=AIMAG(Z(J))
      XP1(J)=.1*XP(J)
   14 CONTINUE
      CALL MINV(XP1,N,D,LA,LB)
      DO 25 J=1,NZ
      XP1(J)=.1*XP1(J)
   25 CONTINUE
      DO 15 K=1,N5
      READ(1,16)(VR(I),I=1,N)
   16 FORMAT(7E11.4)
      WRITE(3,17)(VR(I),I=1,N)
   17 FORMAT('0VR'/(1X,7E11.4))
      DO 18 J=1,N
      RV(J)=REAL(VR(J))
      AV(J)=AIMAG(VR(J))
```

```
18 CONTINUE
   S1=0.
   S2=0.
   DO 19 J=1,N
   FI(J)=0.
   J3=(J-1)*N
   DO 20 I=1,N
   J1=J3+I
   FI(J)=FI(J)+XP1(J1)*VR(I)
20 CONTINUE
   RI(J)=REAL(FI(J))
   AI(J)=AIMAG(FI(J))
   S1=S1+ABS(RI(J))
   S2=S2+ABS(AI(J))
19 CONTINUE
   GB2=0.
   DO 26 J=1,N
   GB2=GB2+RV(J)*RI(J)+AV(J)*AI(J)
26 CONTINUE
   GB2=GB2*C1
   IF((S1*S2).NE.0.) GO TO 27
   GB1=GB2
   DO 28 J=1,N
   CUR(J)=RI(J)+AI(J)
28 CONTINUE
   GO TO 29
27 S1=0.
   S2=0.
   S3=0.
   DO 30 J=1,N
   S1=S1+RV(J)*RI(J)
   S2=S2+AV(J)*AI(J)
   S3=S3+RV(J)*AI(J)
30 CONTINUE
   A=(S1-S2)/(2.*S3)
   SA=SQRT(A*A+1.)
   C=-A+SIGN(SA,S3)
   GB1=C1*(S1+C*S3)
   DO 31 J=1,N
   CUR(J)=RI(J)+C*AI(J)
31 CONTINUE
29 S1=0.
   J1=1
   DO 32 J=1,N
   S2=ABS(CUR(J))
   IF(S2-S1) 32,32,24
24 S1=S2
   J1=J
32 CONTINUE
   S1=1./CUR(J1)
   DO 33 J=1,N
   CUR(J)=CUR(J)*S1
33 CONTINUE
   WRITE(3,34) GB1,GB2
34 FORMAT('0',4X,'GB1',8X,'GB2'/1X,2E11.4)
   WRITE(3,35)(CUR(J),J=1,N)
35 FORMAT('OREAL CURRENT FOR MAXIMUM GAIN-QUALITY RATIO'/(1X,10F8.4))
   WRITE(3,36)(FI(J),J=1,N)
36 FORMAT('OCOMPLEX CURRENT FOR MAXIMUM GAIN-QUALITY RATIO'/(1X,7E11.
  14))
15 CONTINUE
   STOP
   END
```

```
/*
//GO.FT06F001 DD DSNAME=EE0034.REV1,DISP=OLD,UNIT=2314,                X
//             VOLUME=SER=SU0004,DCB=(RECFM=VS,BLKSIZE=2596,LRECL=2592)
//GO.SYSIN DD *
 30  1  2 0.1039861E+00
 0.3666E+00 0.3734E-04-0.9808E+00-0.1786E+00-0.9330E+00-0.3514E+00-0.8550E+00
-0.5129E+00-0.7492E+00-0.6577E+00-0.6193E+00-0.7813E+00-0.4693E+00-0.8796E+00
-0.3042E+00-0.9494E+00-0.1292E+00-0.9886E+00 0.5001E-01-0.9957E+00 0.2276E+00
-0.9706E+00 0.3978E+00-0.9142E+00 0.6216E+00-0.1063E+01 0.6200E+00-0.1323E+01
 0.4122E+00-0.1402E+01 0.1949E+00-0.1448E+01-0.2699E-01-0.1461E+01-0.2482E+00
-0.1440E+01 0.1143E+00 0.1038E+00 0.7165E+00 0.1575E+01 0.8761E+00 0.1492E+01
 0.1026E+01 0.1393E+01 0.1165E+01 0.1279E+01 0.1292E+01 0.1151E+01 0.1404E+01
 0.1011E+01 0.1502E+01 0.8596E+00 0.1583E+01 0.6991E+00 0.1647E+01 0.5311E+00
 0.1693E+01 0.3573E+00 0.1721E+01 0.1796E+00
/*
//
```

SAMPLE PRINTED OUTPUT

```
 N  N5 N6       BK
 30  1  2 0.1039861E+00

VR
 0.3666E+00 0.3734E-04-0.9808E+00-0.1786E+00-0.9330E+00-0.3514E+00-0.8550E+00
-0.5129E+00-0.7492E+00-0.6577E+00-0.6193E+00-0.7813E+00-0.4693E+00-0.8796E+00
-0.3042E+00-0.9494E+00-0.1292E+00-0.9886E+00 0.5001E-01-0.9957E+00 0.2276E+00
-0.9706E+00 0.3978E+00-0.9142E+00 0.6216E+00-0.1063E+01 0.6200E+00-0.1323E+01
 0.4122E+00-0.1402E+01 0.1949E+00-0.1448E+01-0.2699E-01-0.1461E+01-0.2482E+00
-0.1440E+01 0.1143E+00 0.1038E+00 0.7165E+00 0.1575E+01 0.8761E+00 0.1492E+01
 0.1026E+01 0.1393E+01 0.1165E+01 0.1279E+01 0.1292E+01 0.1151E+01 0.1404E+01
 0.1011E+01 0.1502E+01 0.8596E+00 0.1583E+01 0.6991E+00 0.1647E+01 0.5311E+00
 0.1693E+01 0.3573E+00 0.1721E+01 0.1796E+00

    GB1         GB2
 0.1063E+00 0.1592E+00

REAL CURRENT FOR MAXIMUM GAIN-QUALITY RATIO
  0.3773  0.1698 -0.0015 -0.1454 -0.2611 -0.3496 -0.4126 -0.4524 -0.4711 -0.4726
 -0.4602 -0.4390 -0.4131 -0.3734 -0.3175 -0.2340 -0.1101  0.0678  0.3279  0.5807
  0.7566  0.8804  0.9584  0.9971  1.0000  0.9710  0.9117  0.8233  0.7063  0.5613

COMPLEX CURRENT FOR MAXIMUM GAIN-QUALITY RATIO
 0.1066E-01-0.4325E-03 0.7057E-02-0.2188E-02 0.4475E-02-0.3982E-02 0.2647E-02
-0.5790E-02 0.1517E-02-0.7544E-02 0.9928E-03-0.9186E-02 0.9806E-03-0.1067E-01
 0.1387E-02-0.1198E-01 0.2114E-02-0.1306E-01 0.3068E-02-0.1394E-01 0.4148E-02
-0.1460E-01 0.5251E-02-0.1507E-01 0.6267E-02-0.1535E-01 0.6736E-02-0.1482E-01
 0.6925E-02-0.1365E-01 0.7113E-02-0.1183E-01 0.7516E-02-0.9245E-02 0.8347E-02
-0.5751E-02 0.9911E-02-0.9462E-03 0.1178E-01 0.3414E-02 0.1338E-01 0.6187E-02
 0.1480E-01 0.7879E-02 0.1599E-01 0.8680E-02 0.1693E-01 0.8771E-02 0.1755E-01
 0.8291E-02 0.1782E-01 0.7371E-02 0.1764E-01 0.6114E-02 0.1696E-01 0.4619E-02
 0.1567E-01 0.2975E-02 0.1368E-01 0.1277E-02
```

VI. PATTERN SYNTHESIS

A program has been written to calculate β and α_n appearing in (34) and (35). The activity on data sets 1 (punched card input) and 6 (direct access input-output) is as follows.

```
      READ(1,4) N, NT, N6, N7, N8
4     FORMAT(20I3)
      REWIND 6
      NTN = N*NT
      NZ = N8*N
      SKIP N6 RECORDS ON DATA SET 6
      READ(6)(VR(I), I = 1, NTN)
      SKIP N7 RECORDS ON DATA SET 6
      READ(6)(FI(I), I = 1, NZ)
      READ(1,4)M,M9
      READ(1,4)(NE(I), I = 1, M)
      READ(1,4)(NM(I), I = 1, N9)
      READ(1,7)(RE(I), I = 1, M)
7     FORMAT(7E11.4)
      READ(1,7)(AE(I), I = 1, M)
```

A slight modification of the program of Section IV has stored receiver excitations VR for at least all the M different unit plane waves corresponding to E_o^m of (36). The receiver excitation (53) for the Jth unit plane wave and the Ith triangular expansion function should be stored in VR((J-1)*N+I). The program of Section III of [20] has stored the eigencurrents FI for the unloaded surface. The M and N9 of the program correspond respectively to M and N of (36). The real and imaginary parts of E_o^m of (36) are read in through RE and AE. The receiver excitation for the (NE(I))th unit plane wave must be used to calculate a far field that can be compared to RE(I) + jAE(I). The (NM(n))th eigencurrent is the nth eigencurrent to be added in the sum (34). The variable NM is necessary because the program of Section III of [20] stores the eigencurrents in order of increasing λ while it may be preferable to do the sum (35) in order of increasing $|\lambda|$.

DO loop 20 stores the real and imaginary parts of the matrix [A] of (38) in RA and AA. If NT > M, RA + jAA has extra rows. If N8 > N9, RA + jAA has extra columns. With RA + jAA thus computed recycling could be obtained if all the logic beyond statement 37 were put in a DO loop. DO loop 45 stores $[\tilde{E}^*][E]$ in EE.

The index J of DO loop 25 corresponds to n in (36). DO loop 26 stores the real and imaginary parts of $[\tilde{A}^*E]$ in AE1 and AE2. DO loop 28 puts the Jth column of $[RE(\tilde{A}^*A)]$ in B according to the symmetric storage mode described in page 4 of [23]. DO loop 32 stores $[Re(\tilde{A}^*A)]$ in BB columnwise. The subroutine MINV [23] inverts BB. DO loop 34 stores $[Re(\tilde{A}^*A)]^{-1}Re[\tilde{A}^*E]$ in T1 and $[Re(\tilde{A}^*A)]^{-1}Im[\tilde{A}^*E]$ in T2. Expressions (43)-(45) are stored in C1, C2, and C3. Since the Fortran supplied subroutine ATAN gives an angle between -90° and 90°, there are two solutions BET(1) and BET(2) to (46). DO loop 46 computes the mean square error (42) for β = BET(K). DO loop 50 stores $[\alpha]$ of (40) in AL. DO loop 52 stores the coefficients of the triangular expansion functions for $\sum_{n=1}^{J} \alpha_n \vec{J}_n$ of (34) in CUR. If the given far electric field E_θ is written

$$E_\theta = \frac{-j\omega\mu e^{-jkr}}{4\pi r} E_o^m$$

where E_o^m is the data RE + jAE, then $e^{j\beta}$ times CURR is the electric current (evaluated at the peaks of the triangular expansion functions) whose far field approximates E_θ. DO loop 54 stores the real and imaginary parts of the approximation to RE + jAE in E1 and E2.

Minimum allocations are given by

```
COMPLEX VR(NT*N)
DIMENSION FI(N8*N), RA(N8*NT), AA(N8*NT),
    NE(M), NM(N9), RE(M), AE(M), AE1(N9),
    AE2(N9), B(N9*(N9+1)/2), BB(N9*N9),
    ML(N9), MM(N9), T1(N9), T2(N9), AL(N9),
    CUR(N), E1(M), E2(M)
```

The sample input data and printed output are for the wire triangle of Fig. 1 with E_θ of (48) evaluated at the 15 angles 10° to 170° in steps of 10° except for 50° and 130°. The receiver excitations VR have been calculated at the 73 angles 0° to 180° in steps of 2.5° and stored in record 4 of data set 6 whereas the eigencurrents of the unloaded surface have been stored on record 5 of data set 6.

LISTING OF PROGRAM FOR PATTERN SYNTHESIS

```
//              (0034,EE,3,2),'MAUTZ,JOE',REGION=140K
// EXEC SSPCLG,PARM.FORT='MAP'
//FORT.SYSIN DD *
      COMPLEX VR(2190),U2
      DIMENSION FI(900),RA(584),AA(584),NE(30),NM(30),RE(30),AE(30)
      DIMENSION AE1(30),AE2(30),B(465),BB(900),ML(30),MM(30),T1(30)
      DIMENSION T2(30),BET(2),ER(2),AL(30),CUR(30),E1(30),E2(30)
      P2=3.141593/2.
      READ(1,4) N,NT,N6,N7,N8
    4 FORMAT(20I3)
      WRITE(3,5) N,NT,N6,N7,N8
    5 FORMAT('0  N NT N6 N7 N8'/1X,5I3)
      REWIND 6
      NTN=N*NT
      NZ=N8*N
      IF(N6) 11,11,12
   12 DO 13 J=1,N6
      READ(6)
   13 CONTINUE
   11 READ(6)(VR(I),I=1,NTN)
      WRITE(3,14)(VR(I),I=1,3)
   14 FORMAT('0VR'/(1X,6E11.4))
      J1=IABS(N7)
      IF(N7) 15,16,17
   15 DO 18 J=1,J1
      BACKSPACE 6
   18 CONTINUE
      GO TO 16
   17 DO 19 J=1,J1
      READ(6)
   19 CONTINUE
   16 READ(6)(FI(I),I=1,NZ)
      WRITE(3,24)(FI(I),I=1,7)
   24 FORMAT('0FI'/(1X,7E11.4))
      DO 20 J=1,N8
      J1=(J-1)*NT
      J6=(J-1)*N
      DO 21 I=1,NT
      J3=(I-1)*N
```

```
      J2=J1+I
      U2=0.
      DO 22 K=1,N
      J4=J3+K
      J5=J6+K
      U2=U2+VR(J4)*FI(J5)
   22 CONTINUE
      RA(J2)=REAL(U2)
      AA(J2)=AIMAG(U2)
   21 CONTINUE
   20 CONTINUE
      WRITE(3,36)(RA(I),I=1,7)
   36 FORMAT('ORA'/(1X,7E11.4))
      WRITE(3,37)(AA(I),I=1,7)
   37 FORMAT('OAA'/(1X,7E11.4))
      READ(1,4) M,N9
      WRITE(3,38) M,N9
   38 FORMAT('0 M  N9'/1X,2I3)
      READ(1,4)(NE(I),I=1,M)
      WRITE(3,9)(NE(I),I=1,M)
    9 FORMAT('ONE'/(1X,20I3))
      READ(1,4)(NM(I),I=1,N9)
      WRITE(3,23)(NM(I),I=1,N9)
   23 FORMAT('ONM'/(1X,20I3))
      READ(1,7)(RE(I),I=1,M)
    7 FORMAT(7E11.4)
      WRITE(3,8)(RE(I),I=1,M)
    8 FORMAT('ORE'/(1X,7E11.4))
      READ(1,7)(AE(I),I=1,M)
      WRITE(3,29)(AE(I),I=1,M)
   29 FORMAT('OAE'/(1X,7E11.4))
      EE=0.
      DO 45 J=1,M
      EE=EE+RE(J)*RE(J)+AE(J)*AE(J)
   45 CONTINUE
      J3=0
      DO 25 J=1,N9
      J1=(NM(J)-1)*NT
      AE1(J)=0.
      AE2(J)=0.
      DO 26 I=1,M
      J2=J1+NE(I)
      AE1(J)=AE1(J)+RE(I)*RA(J2)+AE(I)*AA(J2)
      AE2(J)=AE2(J)+AE(I)*RA(J2)-RE(I)*AA(J2)
   26 CONTINUE
      DO 27 I=1,J
      J3=J3+1
      B(J3)=0.
      J6=(NM(I)-1)*NT
      DO 28 K=1,M
      J4=J1+NE(K)
      J5=J6+NE(K)
      B(J3)=B(J3)+RA(J4)*RA(J5)+AA(J4)*AA(J5)
   28 CONTINUE
   27 CONTINUE
      J8=0
      DO 32 K=1,J
      J4=(K-1)*J
      DO 33 L=1,K
```

```
      J8=J8+1
      J5=J4+L
      J6=(L-1)*J+K
      BB(J5)=B(J8)
      BB(J6)=BB(J5)
   33 CONTINUE
   32 CONTINUE
      CALL MINV(BB,J,D,ML,MM)
      DO 34 K=1,J
      T1(K)=0.
      T2(K)=0.
      J1=(K-1)*J
      DO 35 I=1,J
      J2=J1+I
      T1(K)=T1(K)+BB(J2)*AE1(I)
      T2(K)=T2(K)+BB(J2)*AE2(I)
   35 CONTINUE
   34 CONTINUE
      C1=0.
      C2=0.
      C3=0.
      DO 43 I=1,J
      C1=C1-T1(I)*AE1(I)
      C2=C2-T2(I)*AE2(I)
      C3=C3-T2(I)*AE1(I)
   43 CONTINUE
      C3=C3*2.
      BET(1)=.5*ATAN(C3/(C1-C2))
      BET(2)=BET(1)-SIGN(P2,BET(1))
      WRITE(3,51) J
   51 FORMAT('0',I3,' MODE SOLUTION')
      DO 46 K=1,2
      CS=COS(BET(K))
      SN=SIN(BET(K))
      ER(K)=C1*CS*CS+C2*SN*SN+C3*SN*CS+EE
   46 CONTINUE
      IF(ER(1)-ER(2)) 47,47,48
   47 BETA=BET(1)
      ERR=ER(1)
      GO TO 49
   48 BETA=BET(2)
      ERR=ER(2)
   49 SN=SIN(BETA)
      CS=COS(BETA)
      DO 50 I=1,J
      AL(I)=T1(I)*CS+T2(I)*SN
   50 CONTINUE
      WRITE(3,56) BETA,ERR
   56 FORMAT('0',4X,'BETA',7X,'ERR'/1X,2E11.4)
      WRITE(3,57)(AL(I),I=1,J)
   57 FORMAT('0MODE COEFFICIENTS'/(1X,7E11.4))
      DO 52 K=1,N
      CUR(K)=0.
      DO 53 I=1,J
      J6=K+(NM(I)-1)*N
      CUR(K)=CUR(K)+AL(I)*FI(J6)
   53 CONTINUE
```

```
   52 CONTINUE
      WRITE(3,58)(CUR(I),I=1,N)
   58 FORMAT('0CUR'/(1X,7E11.4))
      DO 54 K=1,M
      S4=0.
      E2(K)=0.
      DO 55 I=1,J
      J6=(NM(I)-1)*NT+NE(K)
      S4=S4+AL(I)*RA(J6)
      E2(K)=E2(K)+AL(I)*AA(J6)
   55 CONTINUE
      E1(K)=CS*S4-SN*E2(K)
      E2(K)=SN*S4+CS*E2(K)
   54 CONTINUE
      WRITE(3,59)(E1(I),I=1,M)
   59 FORMAT('0E1'/(1X,7E11.4))
      WRITE(3,60)(E2(I),I=1,M)
   60 FORMAT('0E2'/(1X,7E11.4))
   25 CONTINUE
      STOP
      END
/*
//GO.FT06F001 DD DSNAME=EE0034.REV1,DISP=OLD,UNIT=2314,                    X
//             VOLUME=SER=SU0004,DCB=(RECFM=VS,BLKSIZE=2596,LRECL=2592)
//GO.SYSIN DD *
 30 73  3  0  8
 15  1
  5  9 13 17 25 29 33 37 41 45 49 57 61 65 69
  2
 0.3420E+00 0.6428E+00 0.8660E+00 0.9848E+00 0.8660E+00 0.6428E+00 0.3420E+00
 0.0000E+00-0.3420E+00-0.6428E+00-0.8660E+00-0.9848E+00-0.8660E+00-0.6428E+00
-0.3420E+00
 0.0000E+00 0.0000E+00 0.0000E+00 0.0000E+00 0.0000E+00 0.0000E+00 0.0000E+00
 0.0000E+00 0.0000E+00 0.0000E+00 0.0000E+00 0.0000E+00 0.0000E+00 0.0000E+00
 0.0000E+00
/*
//
```

SAMPLE PRINTED OUTPUT

```
  N NT N6 N7 N8
 30 73  3  0  8

VR
 0.5157E+00 0.3891E-01 0.5053E+00 0.1029E+00 0.4746E+00 0.2017E+00

FI
 0.9240E+00 0.9463E+00 0.9678E+00 0.9849E+00 0.9959E+00 0.1000E+01 0.9969E+00

RA
 0.1128E+02 0.1129E+02 0.1131E+02 0.1134E+02 0.1139E+02 0.1144E+02 0.1150E+02

AA
 0.1625E+01 0.1606E+01 0.1549E+01 0.1454E+01 0.1322E+01 0.1150E+01 0.9399E+00

 M  N9
 15  1
```

```
NE
  5  9 13 17 25 29 33 37 41 45 49 57 61 65 69

NM
  2

RE
 0.3420E+00 0.6428E+00 0.8660E+00 0.9848E+00 0.8660E+00 0.6428E+00 0.3420E+00
 0.0000E+00-0.3420E+00-0.6428E+00-0.8660E+00-0.9848E+00-0.8660E+00-0.6428E+00
-0.3420E+00

AE
 0.0000E+00 0.0000E+00 0.0000E+00 0.0000E+00 0.0000E+00 0.0000E+00 0.0000E+00
 0.0000E+00 0.0000E+00 0.0000E+00 0.0000E+00 0.0000E+00 0.0000E+00 0.0000E+00
 0.0000E+00

  1 MODE SOLUTION

    BETA        ERR
 0.1571E+01 0.5168E+01

MODE COEFFICIENTS
 0.1631E-01

CUR
-0.2539E-06 0.3520E-02 0.6767E-02 0.9728E-02 0.1226E-01 0.1425E-01 0.1562E-01
 0.1631E-01 0.1629E-01 0.1556E-01 0.1417E-01 0.1217E-01 0.9662E-02 0.6623E-02
 0.3378E-02 0.9423E-07-0.3378E-02-0.6623E-02-0.9661E-02-0.1217E-01-0.1417E-01
-0.1556E-01-0.1629E-01-0.1631E-01-0.1562E-01-0.1425E-01-0.1226E-01-0.9728E-02
-0.6767E-02-0.3520E-02

E1
 0.7580E-01 0.1479E+00 0.2108E+00 0.2564E+00 0.2575E+00 0.2010E+00 0.1105E+00
-0.1012E-06-0.1105E+00-0.2010E+00-0.2575E+00-0.2564E+00-0.2108E+00-0.1479E+00
-0.7580E-01

E2
-0.2111E-01-0.5115E-01-0.9732E-01-0.1631E+00-0.3375E+00-0.4217E+00-0.4815E+00
-0.5032E+00-0.4815E+00-0.4217E+00-0.3375E+00-0.1631E+00-0.9732E-01-0.5115E-01
-0.2111E-01
```

VII. SPARSELY LOADED SCATTERERS

A program has been written to compute $[I]_2$ of (51) and [XL] of (52). The activity on data sets 1 (punched card input) and 6 (direct access input-output) is as follows.

```
      READ(1,11) N, N6
11    FORMAT(20I3)
      NZ = N*N
      REWIND 6
      SKIP N6 RECORDS ON DATA SET 6
      READ(6) (Z(I), I = 1, NZ)
      READ(1,11) NL
      READ(1,11) (L(I), I = 1, N)
      READ(1,40) (FI(I), I = 1, N)
40    FORMAT(10F8.4)
```

The impedance matrix Z of order N has been stored on the (N6+1)th record of data set 6 by the program of Section II of [20]. Loads occur at the peaks of the (L(I), I = 1, NL)th triangular expansion functions. There are no loads at the peaks of the remaining (L(I), I = NL + 1, N)th triangular expansion functions. The real current to be resonated is (FI(L(I)), I = 1, NL) at the peaks of the (L(I))th triangular expansion functions.

DO loop 16 stores in X the reactance matrix arranged so that rows and columns corresponding to load positions come first. The subroutine MINV [23] inverts the matrix $[X]_{22}$ of (50) stored in X22 by DO loop 23. DO loop 25 puts $[X_{21}][I]_1$ of (51) in XI. DO loop 27 stores $[I]_2$ of (51) in T2. DO loop 29 stores $[X_L]$ of (52) in XI. DO loop 32 changes the current FI at the no load positions to $[I]_2$ of (51). DO loop 34 stores in XL the reactive loads arranged in the order of the triangular expansion functions implicit in the input data Z and FI.

Minimum allocations are given by

```
      COMPLEX Z(N*N)
      DIMENSION L(N), FI(N), X(N*N),
          X22((N-NL)**2), LB(N-NL), MB(N-NL),
          XI(N), T2(N-NL), XL(N)
```

The sample input data and printed output are for resonating the minimum Q end-fire current on the wire triangle of Fig. 1 with loads on every other expansion of function.

LISTING OF PROGRAM FOR SPARSELY LOADED SCATTERES

```
//              (0034,EE,3,2),'MAUTZ,JOE',REGION=140K
// EXEC SSPCLG,PARM.FORT='MAP'
//FORT.SYSIN DD *
      COMPLEX Z(900)
      DIMENSION L(30),FI(30),X(900),X22(900),LB(30),MB(30),XI(30)
      DIMENSION T2(30),XL(30)
      READ(1,11) N,N6
   11 FORMAT(20I3)
      WRITE(3,35) N,N6
   35 FORMAT('0  N N6'/1X,2I3)
      NZ=N*N
      REWIND 6
      IF(N6) 36,36,37
   37 DO 13 J=1,N6
      READ(6)
   13 CONTINUE
   36 READ(6)(Z(I),I=1,NZ)
      WRITE(3,38)(Z(I),I=1,3)
   38 FORMAT('0Z'/1X,6E11.4)
      READ(1,11) NL
      WRITE(3,12) NL
   12 FORMAT('0NL'/1X,I3)
      READ(1,11)(L(I),I=1,N)
      WRITE(3,14)(L(I),I=1,N)
   14 FORMAT('0L'/(1X,20I3))
      READ(1,40)(FI(I),I=1,N)
   40 FORMAT(10F8.4)
      WRITE(3,41)(FI(I),I=1,N)
   41 FORMAT('0FI'/(1X,10F8.4))
      NL1=NL+1
      NL2=N-NL
      DO 16 J=1,N
      J1=(J-1)*N
      J4=(L(J)-1)*N
      DO 17 I=1,N
      J2=J1+I
      J5=J4+L(I)
      X(J2)=AIMAG(Z(J5))
   17 CONTINUE
   16 CONTINUE
      J1=0
      DO 23 J=NL1,N
      J2=(J-1)*N
```

```
      DO 24 I=NL1,N
      J1=J1+1
      J3=J2+I
      X22(J1)=X(J3)
   24 CONTINUE
   23 CONTINUE
      CALL MINV(X22,NL2,D,LB,MB)
      J1=0
      DO 25 J=NL1,N
      J1=J1+1
      XI(J1)=0.
      J4=(J-1)*N
      DO 26 I=1,NL
      J2=J4+I
      J3=L(I)
      XI(J1)=XI(J1)+X(J2)*FI(J3)
   26 CONTINUE
   25 CONTINUE
      DO 27 J=1,NL2
      T2(J)=0.
      J2=(J-1)*NL2
      DO 28 I=1,NL2
      J1=J2+I
      T2(J)=T2(J)-X22(J1)*XI(I)
   28 CONTINUE
   27 CONTINUE
      DO 29 J=1,NL
      XI(J)=0.
      J2=(J-1)*N+NL
      DO 30 I=1,NL2
      J1=J2+I
      XI(J)=XI(J)+X(J1)*T2(I)
   30 CONTINUE
      J4=(J-1)*N
      DO 31 I=1,NL
      J1=J4+I
      J3=L(I)
      XI(J)=XI(J)+X(J1)*FI(J3)
   31 CONTINUE
      J3=L(J)
      XI(J)=-XI(J)/FI(J3)
   29 CONTINUE
      J1=0
      DO 32 J=NL1,N
      J3=L(J)
      J1=J1+1
      FI(J3)=T2(J1)
   32 CONTINUE
      WRITE(3,41)(FI(I),I=1,N)
      DO 33 J=NL1,N
      XI(J)=0.
   33 CONTINUE
      DO 34 J=1,N
      J3=L(J)
```

```
      XL(J3)=XI(J)
   34 CONTINUE
      WRITE(3,39)(XL(I),I=1,N)
   39 FORMAT('0XL'/(1X,7E11.4))
      STOP
      END
/*
//GO.FT06F001 DD DSNAME=EE0034.REV1,DISP=OLD,UNIT=2314,                X
//             VOLUME=SER=SU0004,DCB=(RECFM=VS,BLKSIZE=2596,LRECL=2592)
//GO.SYSIN DD *
 30  0
 15
  1  3  5  7  9 11 13 15 17 19 21 23 25 27 29  2  4  6  8 10
 12 14 16 18 20 22 24 26 28 30
-0.0300 -0.0266 -0.0206 -0.0102  0.0063  0.0309  0.0660  0.1147  0.1803  0.2673
 0.3806  0.5258  0.7178  0.8825  0.9707  1.0000  0.9716  0.8837  0.7191  0.5267
 0.3810  0.2672  0.1800  0.1142  0.0655  0.0304  0.0058 -0.0107 -0.0210 -0.0268
/*
//
```

SAMPLE PRINTED OUTPUT

```
  N N6
 30  0

Z
 0.5801E-01-0.5873E+03 0.5810 E-01 0.2657E+03 0.5784E-01 0.3124E+02

NL
 15

L
  1  3  5  7  9 11 13 15 17 19 21 23 25 27 29  2  4  6  8 10
 12 14 16 18 20 22 24 26 28 30

FI
 -0.0300 -0.0266 -0.0206 -0.0102  0.0063  0.0309  0.0660  0.1147  0.1803  0.2673
  0.3806  0.5258  0.7178  0.8825  0.9707  1.0000  0.9716  0.8837  0.7191  0.5267
  0.3810  0.2672  0.1800  0.1142  0.0655  0.0304  0.0058 -0.0107 -0.0210 -0.0268

FI
 -0.0300 -0.0209 -0.0206 -0.0001  0.0063  0.0501  0.0660  0.1471  0.1803  0.3157
  0.3806  0.5803  0.7178  0.8521  0.9707  0.9747  0.9716  0.8530  0.7191  0.5811
  0.3810  0.3158  0.1800  0.1468  0.0655  0.0496  0.0058 -0.0005 -0.0210 -0.0211

XL
 0.2027E+03 0.0000E+00 0.6206E+03 0.0000E+00-0.4060E+04 0.0000E+00-0.6929E+03
 0.0000E+00-0.4022E+03 0.0000E+00-0.2557E+03 0.0000E+00-0.1677E+02 0.0000E+00
 0.4981E+02 0.0000E+00 0.5028E+02 0.0000E+00-0.1615E+02 0.0000E+00-0.2555E+03
 0.0000E+00-0.4038E+03 0.0000E+00-0.6995E+03 0.0000E+00-0.4419E+04 0.0000E+00
 0.6147E+03 0.0000E+00
```

REFERENCES

[1] J. K. Schindler, R. B. Mack, and P. Blacksmith, Jr., "The control of electromagnetic scattering by impedance loading," Proc. IEEE, vol. 53, August 1965, pp. 993-1004.

[2] M. G. Andreasen, "Scattering from cylinders with arbitrary surface impedance," Proc. IEEE, vol. 53, No. 8, August 1965, pp. 812-817.

[3] R. F. Harrington and J. R. Mautz, "Computation of radiation and scattering from loaded bodies of revolution," Scientific Report No. 4, Contract No. F19628-68-C-0180 with Air Force Cambridge Research Laboratories, Bedford, Massachusetts, January 1970.

[4] L. Weinberg, "New techniques for modifying monostatic and multistatic radar cross sections," IEEE Trans. on Antennas and Propagation (Communications), vol. AP-11, November 1963, pp. 717-719.

[5] R. F. Harrington, "Theory of loaded Scatterers," Proc. Inst. Elec. Eng., vol. 111, April 1964, pp. 617-623.

[6] Y. Y. Hu, "Back-scattering cross section of a center-loaded cylindrical antenna," IRE Trans. on Antennas and Propagation, vol. AP-6 January 1958, pp. 140-148.

[7] R. F. Harrington and J. R. Mautz, "Straight wires with arbitrary excitation and loading," IEEE Trans. on Antennas and Propagation, vol. AP-15, July 1967, pp. 502-515.

[8] R. F. Harrington and J. L. Ryerson, "Electromagnetic scattering by loaded wire loops," Radio Science, vol. 1 (New series), March 1966, pp. 347-352.

[9] R. F. Harrington and J. R. Mautz, Electromagnetic behavior of circular wire loops with arbitrary excitation and loading," Proc. Inst. Elect. Eng., vol. 115, January 1968, pp. 68-77.

[10] K. M. Chen and V. Liepa, "Minimization of the backscattering of a cylinder by central loading," IEEE Trans. on Antennas and Propagation, vol. AP-12, September 1964, pp. 576-582.

[11] K. M. Chen, "Minimization of backscattering of a cylinder by double loading," IEEE Trans. on Antennas and Propagation, vol. AP-13, March 1965, pp. 262-270.

[12] J. L. Lin and K. M. Chen, "Minimization of backscattering of a loop by impedance loading-theory and experiment," IEEE Trans. on Antennas and Propagation, vol. AP-16, May 1968, pp. 299-304.

[13] R. F. Harrington, "Small resonant scatterers and their use for field measurements," IRE Trans. on Microwave Theory and Techniques, vol. MTT-10, No. 3, pp. 165-174, May 1962.

[14] R. J. Garbacz and R. H. Turpin, "A generalized expansion for radiated and scattered fields," IEEE Trans. on Antennas and Propagation, vol. AP-19, May 1971, pp. 348-358.

[15] R. J. Garbacz, "A generalized expansion for radiated and scattered fields," Ph.D. Dissertation, The Ohio State University, 1968.

[16] R. F. Harrington and J. R. Mautz, "Theory of characteristic modes for conducting bodies," IEEE Trans. on Antennas and Propagation, vol. AP-19, September 1971.

[17] R. F. Harrington and J. R. Mautz, "Theory and computation of characteristic modes for conducting bodies," Scientific Report No. 9, Contract No. F19628-68-C-0180 with Air Force Cambridge Research Laboratories, Bedford, Massachusetts, December 1970.

[18] R. F. Harrington and J. R. Mautz, "Computation of characteristic modes for conducting bodies," IEEE Trans. on Antennas and Propagation, vol. AP-19, September 1971.

[19] J. R. Mautz and R. F. Harrington, "Computer programs for characteristic modes of bodies of revolution, "Scientific Report No. 10, Contract No. F19628-68-C-0180 with Air Force Cambridge Research Laboratories, Bedford, Massachusetts, January 1971.

[20] J. R. Mautz and R. F. Harrington, "Computer programs for characteristic modes of wire objects," Scientific Report No. 11, Contract No. F19628-68-C-0180 with Air Force Cambridge Research Laboratories, Bedford, Massachusetts, March 1971.

[21] R. F. Harrington ,"Field Computation by Moment Methods," The Macmillan Co., New York, 1968.

[22] H. H. Chao and B. J. Strait, "Computer programs for radiation and scattering by arbitrary configurations of bent wires," Scientific Report No. 7, Contract No. F19628-68-C-0180 with Air Force Cambridge Research Laboratories, Bedford, Massachusetts, September 1970.

[23] IBM System/360 Scientific Subroutine Package (360A-CM-03X) Version III, Programmer's Manual.